THE JOURNAL OF PHYSICAL CHEMISTRY C

Article

Cite This: J. Phys. Chem. C 2018, 122, 25314−25330

pubs.acs.org/JPCC

Seeking a Structure−Function Relationship for γ-Al_2O_3 Surfaces

Muhammed Acikgoz,*[,†] Jaren Harrell,[†] and Michele Pavanello*

Department of Chemistry, Rutgers University, Newark, New Jersey 07102, United States

Supporting Information

ABSTRACT: The surface of γ-Al_2O_3 is perhaps the most exploited surface in chemistry. It is used as a catalyst and as a catalyst support. Its porosity is often evoked as the key quality of this material. However, an atomic-level understanding of this system has yet to be achieved, in most part because of the plethora of microscopic realizations of this surface. The atomic-level understanding of γ-Al_2O_3 surfaces is arguably essential to predict and explain how catalytic and catalytic support properties arise. In this work we aim to characterize the influence of various surface formations that we induce in several surface models (e.g., dehydrated, partially hydroxylated, and terminated with aluminum atoms) by carrying out pseudopotential DFT simulations. By computing surface electronic density of states, $OH/H_2O/H_2$ binding energy, and work functions, we extract a picture of the effects that varying surface coverages, surface adsorbents, and the surrounding environment have on stability, morphology, and position of the Fermi level (via the work function). We show that surface morphological variations can induce significant changes in work function and surface dipole, particularly in regards to the surface oxidation level. Our results offer a new perspective on the surface morphology of γ-Al_2O_3 aimed at understanding structure−electronic properties relationships, e.g., by shedding light on a nonadditive/synergistic effect for water adsorption on γ-Al_2O_3.

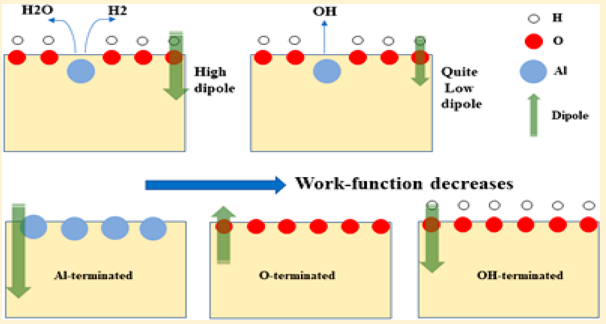

1. INTRODUCTION

Alumina, Al_2O_3, is a versatile material that is chemically inert, insulating, and has high electronic resistance.[1−3] Some of the most studied, preferable, and sought-after aluminas occur at low temperatures and have desirable surface properties, such as high surface area and catalytic activity.[4] Among the many phases of Al_2O_3 (such as γ, χ, κ, δ, η, θ), γ-Al_2O_3 stands out as having the broadest applications.[2,3,5−7] Due to its high degree of porosity, surface area, mechanical strength, insulator properties, integrity, and cost effectiveness,[8,9] γ-Al_2O_3 is perhaps the most important, with direct application as a catalyst and catalyst support in many industries such as oil refineries, automotive, and electroluminescent displays.[3,6,7,10]

The fundamental aspect of preparation and synthesis steps as well as the reactivity of the eventual catalyst is based on the control of surface properties of γ-Al_2O_3.[11,12] For these reasons, characterization of γ-Al_2O_3 is of high priority. Years of research, experimental and theoretical, have carried out comprehensive characterizations of the surface of γ-Al_2O_3 and attempted to understand the mechanism and behavior as a catalyst or catalyst support. To date, however, the structure of γ-Al_2O_3 is still debated, especially with regard to how surface properties are developed. It is essential to continue studying γ-Al_2O_3 with different crystal morphologies to shed light on its structure−function relationships. The debate stems from the fact that the bulk crystal structure of γ-Al_2O_3 has multiple incongruent characterizations, but the two more common descriptions are (1) a defective (nonstoichiometric) or nonspinel structure, with tetragonal distortions, and (2) a cubic spinel crystal structure containing a cubic oxygen sublattice that can be face-centered cubic or cubic close-packed.[7,13−16] Some have also presented γ-Al_2O as a dual-phase material containing tetragonal and cubic characteristics.[6,16,17] Others debate if hydrogen and/or OH is contained within the bulk, consider the percent of Al with tetrahedral and octahedral coordination, or examine the distribution of naturally occurring vacancies/defect sites. The majority of studies (both theoretical and experimental) conclude that the bulk does not contain either hydrogen or hydroxyls but that instead the hydroxyls migrate to the surface during the ceramic processes employed in the synthesis of γ-Al_2O_3.[17−20] However, Wefers and Misra[21] pointed out a transitional form of γ-Al_2O_3 in a wide range of temperature (450−780 K) that is too low to remove all hydrogen from the bulk. Moreover, a non-negligible hydrogen content was reported, even though the material was heated to 873 K for 1 h.[22] One can see the detailed discussion of the hydrogen content of γ-Al_2O_3 in the review paper by Sohlberg et al.[23]

Past research has presented that 25−40% of Al atoms in the bulk of γ-Al_2O_3 are tetrahedrally coordinated and 60−75% are instead octahedrally coordinated[6,7,11,17,18,24−26] The locations of vacancies are disputed as being at only octahedral or tetrahedral Al sites or distributed between both sites.[2,4,13,15,27] Theoretical studies on the vacancy sites by Menendez-Proupin

Received: July 7, 2018
Revised: October 1, 2018
Published: October 9, 2018

DOI: 10.1021/acs.jpcc.8b06506
J. Phys. Chem. C 2018, 122, 25314−25330

and Gutierrez[28] as well as Paglia et al.[6,16,20,29] and Taniike et al.[30] found that the lowest energy structure had the vacancies in their model unit cells be in the octahedral cation sites with the longest distance between the vacancies. None of the vacancies were situated on the surface due to large reconstruction that has atoms collapsing into the vacancy.[31] The poor degree of crystallinity and inconsistent results are at the core of the difficulty and elusiveness of the γ-Al_2O_3 structure determination.

Defining a model surface of γ-Al_2O_3 has been equally laborious and diverse as trying to portray the bulk crystal structure, because of the nonhomogeneity of prepared samples. Investigations of the surface, especially hydrated surfaces, have proposed explanations about how catalytic activity arises. Metal oxides like γ-Al_2O_3, at ambient temperature and pressure, are typically covered by a layer of water molecules by molecular adsorption or chemisorption. This also induces the formation of surface hydroxyl groups in variable concentration depending on the surfaces' microscopic morphology and temperature.[27,4,32−39] Dabrowski et al.[33] have shown that the activity of γ-Al_2O_3 as a catalyst support is influenced by the degree of hydration of the surface. Al-Abadleh et al.[34] have verified that uptake of water on the surface interferes with γ-Al_2O_3 reactivity and performance.

Studies of hydroxyl groups on γ-Al_2O_3 surfaces have shown that hydroxyls have different vibrational frequencies depending on the local environment, such as neighboring hydroxyls, surface coverage, and the acidic character of surrounding open sites.[11,33,38,40,41] Experimental data and theoretical calculations provided vibrational frequencies of hydroxyls on various surface terminations. They have found there can be five different hydroxyl groups and as many as seven depending on environmental and surface conditions.[14,20,34,42,43] These studies have successfully identified some of the characteristic peaks in the IR spectrum of γ-Al_2O_3, but some features are still not explained regarding bridged hydroxyl groups. Studies have illustrated that water/hydroxyl removal is essential for the development of catalytic surface properties, so further examinations of surface hydroxyls will provide more information.[43,44]

Several mechanisms of catalytic activity by bare γ-Al_2O_3 have been proposed, i.e., one by the elimination of water as the temperature increases, that create open surface sites,[27,33,45−48] and another attributes catalytic activity to the strain of the surface induced by water being expelled during dehydration at calcination; the released strain would be the motivating force for catalysis.[45] At high temperatures, some surfaces are reported to be completely dehydrated, while Hendriksen et al.[49] have seen that even at 1000 °C hydroxyl groups are still present on the surface. Experimental and theoretical evidence show that the surface possesses acid−base properties emerging from dehydration.[37,42,46,50] Tetrahedral surface aluminum atoms are said to have stronger Lewis acidity than surface octahedral aluminum atoms.[24,51,52] Surfaces examined for Lewis acid/base, Bronsted acid/base, and open surface sites constitute another explanation behind the driving force for catalytic properties.[40,47,53,54] Additional research has stated that dehydroxylation can cause the reorganization of surface charges.[54]

Water plays an important role in the morphology and stability of γ-Al_2O_3. A nonadditive/synergistic effect for water adsorption was discovered related to hydroxylation of four-coordinate Al sites of (100) termination in γ-Al_2O_3.[55] Experimental evidence for the mechanism of synergistic effect of adsorption and reaction between SO_2 and NO_2 was provided on γ-Al_2O_3 surfaces.[56] Some other synergistic effects were also reported for Cl_2, NO_2, and SO_2 once they react on γ-Al_2O_3 surface under humid condition.[57] However, structure−function relations under these synergistic effects have not been fully explored/understood. Thus, the efforts are worthy for understanding the origin of nonadditive/synergistic effects in γ-Al_2O_3 as a supported catalyst combining multiple functionalities.[58]

In this work, we carry out a computational study of the (001) aluminum and oxygen-terminated surface models that are generated from a γ-Al_2O_3 bulk model. We focus on the binding energy of absorbed species such as H_2O, OH, and H_2 and the associated shifts in the surface work function. As we have mentioned previously, dehydration of γ-Al_2O_3 has an important role in catalytic activity. Thus, we study the surface effects as H_2O and/or OH molecules are removed from a hydrated surface. The resulting work offers a new perspective and a general picture of the surface morphology of γ-Al_2O_3 as well as the morphology−electronic properties relationship that has not been investigated before.[11,22,37,46,59,60]

Several studies have already pointed out that the (001), which coincides with the (111) cut of the cubic spinel structure, surface cuts are thermodynamically more stable than others.[3,15,31] Thus, we investigate more than one type of surface models on the (001) surface which are likely exposed when γ-Al_2O_3 is used in real-life applications.[43,44] We also analyze trends between the partial density of states (PDOS) and work functions as well as the vibrational frequencies of these surfaces. Previous investigations on γ-Al_2O_3 have exposed the importance of surface adsorbents, OH, H_2O, and H_2, on support stability during both catalyst preparation and implementation. However, the relation between surrounding surface environment and surface dipole moment is not fully understood yet. Thus, one of our goals in this study is to clearly demonstrate the change of surface dipole moment with the influence of adsorbent removal on the most realistic γ-Al_2O_3 surfaces.

2. COMPUTATIONAL DETAILS

We model γ-Al_2O_3 with density functional theory (DFT) in the plane wave pseudopotential implementation. Specifically, we employ the Quantum ESPRESSO software.[61]

Table 1. Abbreviations for γ-Al_2O_3 Models Having Two Different Total Number of Atoms and Surface Areas

	small cell (31 Å^2)	supercell (125 Å^2)
bulk	GA0	GA0z
dehydrated/metal term. surf.	GA1	GA1z
oxygen term. surf.	GA2	GA2z
hydrated surf.	GA3	GA3z
removed OH	GA3−OH	GA3z−OH
removed H_2O	GA3−H_2O	GA3z−H_2O
removed H_2	GA3−H_2	GA3z−H_2

In all calculations, a cutoff of 50 Ry for the wave functions kinetic energy and 500 Ry kinetic energy cutoff for the charge density and potential energy were employed, along with a very small Gaussian smearing of σ = 0.0001 Ry to generate the conduction band for PDOS plots. The calculations also had a mixing β of 0.10 and a k-point sampling at the Γ-point for

DOI: 10.1021/acs.jpcc.8b06506
J. Phys. Chem. C 2018, 122, 25314−25330

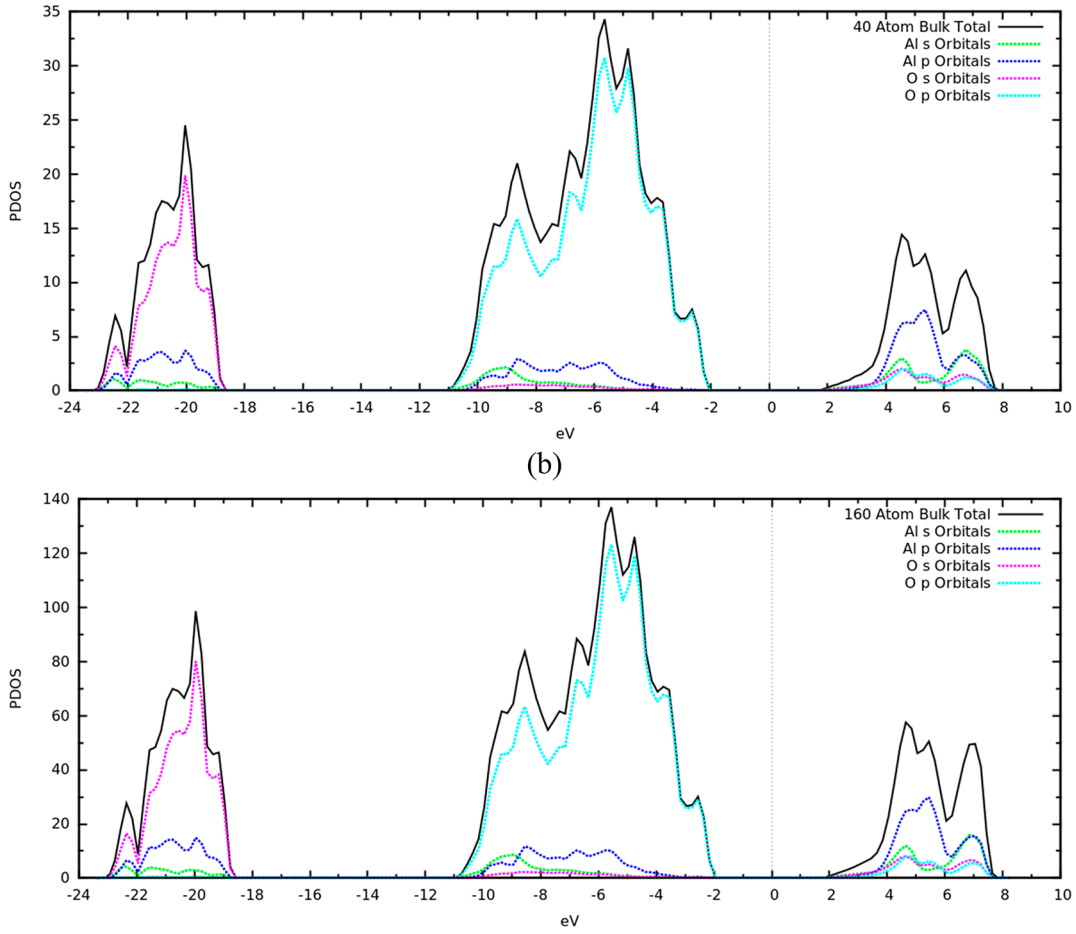

Figure 1. DOS of (a) GA0 and (b) GA0z bulk γ-Al_2O_3. The Fermi energy is set to zero. DOS in arbitrary units.

geometry optimizations and 4 × 4 × 1 for all single-point, self-consistent field (SCF) calculations. An additional non-self-consistent field (NSCF) was employed to generate a smother partial density of states (P/DOS) done on an even 8 × 8 × 8 *k*-point grid. The calculated Fermi levels were set to zero for all (partial) density of state plots. Phonon calculations were computed on the 40-atom small cell (will later be described) to generate vibrational frequencies carried out with fixed occupations (no smearing). This was done at this size model due to the high computational cost when using a model with a high number of total atoms. The wave function kinetic energy cutoff for phonon calculation was 70 Ry on a 2 × 2 × 1 *k*-point grid.

2.A. Bulk Model Structure. We have chosen a hydrogen-free bulk structure model as one of the possible choices for γ-Al_2O_3. It is worth to note that different spinel structures involving hydrogen were proposed, such as a HAl_5O_8 composition by Sohlberg et al.[19] as a residual of boehmite; however, it was asserted by Wolverton and Hass[62] and Digne et al.[63] that these bulk structures containing hydrogen were thermodynamically less stable.[30] Our γ-Al_2O_3 model was based on the findings from Gutierrez et al.,[2] Pinto et al.,[7] and Taniike et al.[30] and have been compared to the theoretical and experimental results of Paglia et al.[16,17] The model we used was a 40-atom bulk crystal structure studied by Menéndez-Proupin and Gutiérrez[28] and was calculated on the basis of a non-spinel or so-called defective-spinel model, where small units of the cubic spinel $MgAl_2O_4$ were combined.[17,18,28,64] This structure is also the closest in agreement to experimental NMR and diffraction patterns.[11,28,29,65] The cell was created by replacing Mg atoms with Al and then removing two aluminum atoms for stoichiometry creating vacancies in tetrahedral or octahedral sites. Optimization of the unit cell and lattice parameters was calculated by Pinto et al.,[7] Paglia et al.,[17] and Menéndez-Proupin and Gutiérrez[28] for vacancy locations with the lowest energy. They concluded that the vacancies, within the cell with the lowest minimum energy for their γ-Al_2O_3 models, were located in two octahedral positions. On the basis of the reported research, we believe this model of γ-Al_2O_3 to be the best representation of a single crystal.

Two different-sized bulk unit cells were used in this research to construct and analyze the surface of γ-Al_2O_3. The initial bulk (used from the literature) contains 40 atoms with a cell volume of 421 Å^3, and a bulk supercell consisting of 160 atoms having a volume of 1684 Å^3 was created to verify the smaller model results.

2.B. Surface Model Structure. The optimized bulk structures, the small cell and supercell, and atomic positions were used to generate surface slabs of the (001) plane possessing the same periodicity of spacing in *x* and *y* directions. A quite thick vacuum thickness of 15 Å above the surface was added between two periodically repeated slabs. Since each slab is symmetric on both sides of the slab and the utilized vacuum layer is sufficiently thick, unphysical electrostatic interactions between the successive slabs can be ignored. Our (001) surface model coordinates to the (110) surface of boehmite and coincides with the (111) plane for the cubic spinel structure.[7,11,66] As shown by Pinto et al.,[7] the (001) and

DOI: 10.1021/acs.jpcc.8b06506
J. Phys. Chem. C 2018, 122, 25314−25330

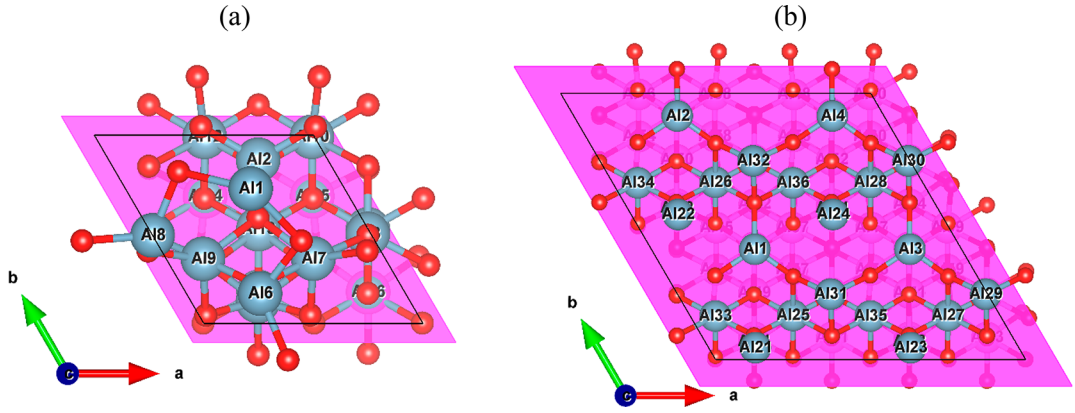

Figure 2. Optimized metal-terminated surface of (a) GA1 and (b) GA1z.

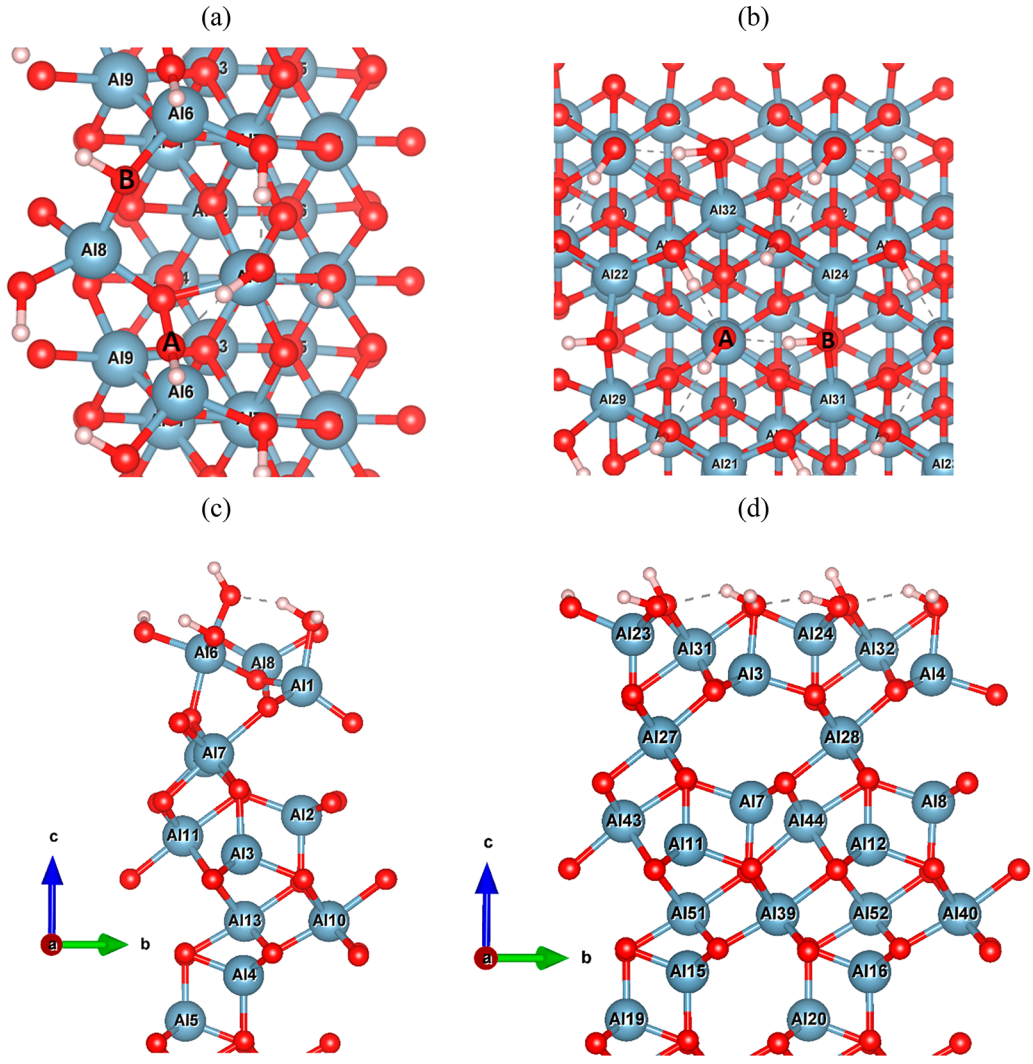

Figure 3. Hydroxyl network on the surface of (a) GA3 and (b) GA3z. Hydroxyls are labeled to indicate the different removal sites. The 100% hydroxylated optimized surface of γ-Al_2O_3: side view of (c) GA3 (small cell) and (d) GA3z (large supercell).

(111) surfaces have lower calculated surface energies than the other surfaces. The detailed description of the terminations regarding (001) surfaces in γ-Al_2O_3 was provided Vijay et al.[15] Different surfaces were created to model the various possibilities of topology exposed in experimental settings. Unlike most, our model slabs are terminated/exposed with Al atoms that are tetrahedrally and octahedrally coordinated and include an aluminum-terminated surface, oxygen-terminated surface, and a completely hydroxylated surface. Fleisher et al.[47,48] also agrees that Al ions can appear on the surface when crystals split at the cation layers that are tetrahedrally and octahedrally coordinated.

Our (001) was an ideal surface with tetrahedral and octahedral aluminum cations and is regarded to have more

DOI: 10.1021/acs.jpcc.8b06506
J. Phys. Chem. C 2018, 122, 25314−25330

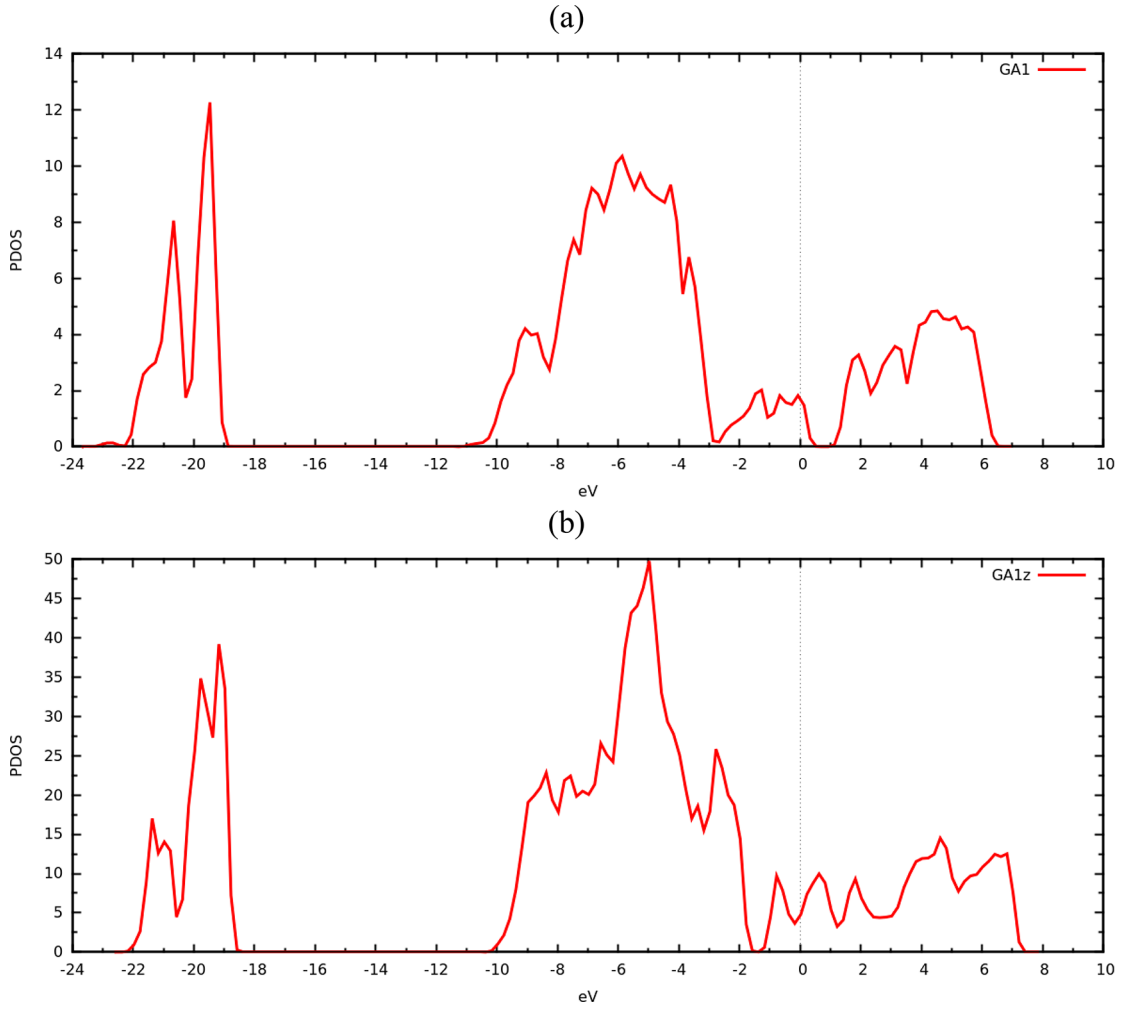

Figure 4. PDOS of the metal-terminated surface for (a) GA1 and (b) GA1z. The Fermi energy is set to zero.

surface activity than other surfaces.[67] This surface will have the maximum amount of open/unsaturated surface sites compared to oxygen-terminated surfaces. The aluminum-terminated surface can be said to be "free of adsorbents" to model a perfect ideal surface of γ-Al_2O_3 at high temperatures (400−1000 °C). In reality, adsorbents and the concentration of adsorbents will vary among *hkl* surfaces and experimental conditions.[25,35,49,68] Previous research on γ-Al_2O_3 about the dehydration of the surface has shown the surface to be never purely dehydrated, even under UHV (ultrahigh vacuum) conditions; others, however, have shown that γ-Al_2O_3 can be free of adsorbents when heated at very high temperatures.[1,30,34,37,46,69,70] It is believed that both cases are feasible. Different *hkl* surfaces of Al_2O_3 will display different properties. Our hydroxylated surface model will be used to show the effects of hydroxylation and binding energy of adsorbents such as OH, H_2O, and H_2. For easy clarifications of models, abbreviations are given in Table 1. Input files with the given structures are accumulated in the Supporting Information (SI).

The bottom layer of the slab was passivated with hydrogen atoms when necessary to maintain a neutral/stoichiometric slab for the hydroxylated surface models. The excess hydrogens of the hydroxyls have been passivated for the sake of neutrality/stoichiometry by adding the same number hydrogens at the bottom layer. Thus, this passivation balanced the dipole between the surface and bottom of the structure. Maintaining a neutral cell will allow for optimizations to not account for the charge and get false minimum energies.

3. RESULTS

3.A. Bulk. Both geometry optimizations of our bulk cell structures had their cell parameters fixed while the minimum energy structures were computed. There are two different types of aluminum atoms coordinating in the bulk. First, is a tetrahedral site that is coordinated to four oxygen atoms, and the second is an octahedral Al atom, coordinated to six oxygen atoms.

The bonds lengths between Al and O atoms vary widely throughout the cell depending on coordination and proximity to a vacancy site. The 40-atom bulk bond lengths overall are on average marginally shorter than the bond lengths in the 160-atom bulk, which range from 1.80 to 1.98 Å for octahedral aluminum atoms and 1.74 to 1.84 Å for tetrahedral Al atoms. When Al−O bonds are next to a defect/vacancy, the bond lengths decrease.

The density of states (DOS) and partial density of states (PDOS) were calculated for each bulk structure. The computed DOS of GA0 has a band gap of 4 eV, the valence band region is from −11 to −2 eV, and the conduction bandwidth is between 2 and 8 eV, as seen in Figure 1a. The band gap is the same value that Gutierrez et al.[2] calculated, which we know is smaller than the experimental value of 8.7

DOI: 10.1021/acs.jpcc.8b06506
J. Phys. Chem. C 2018, 122, 25314−25330

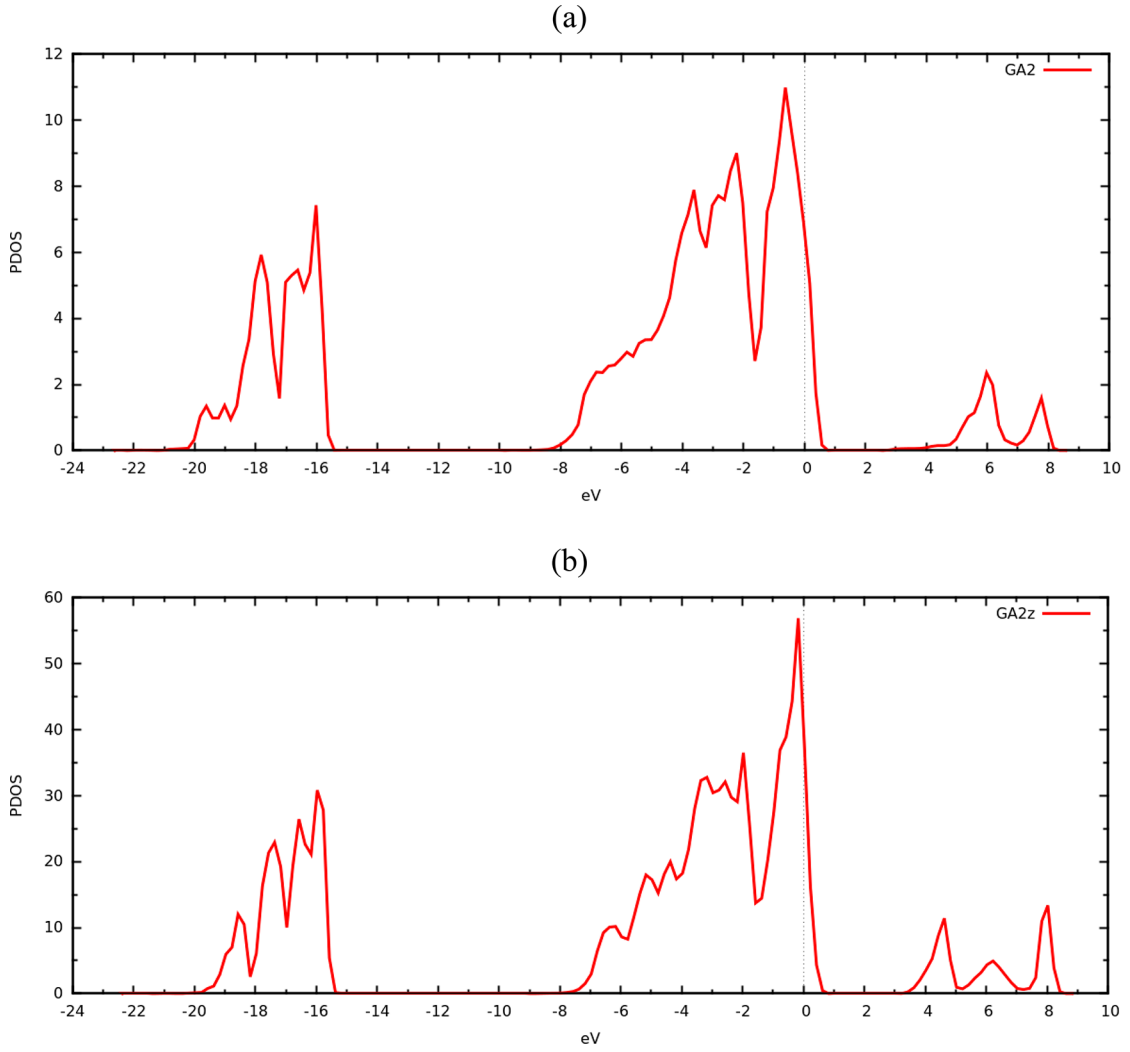

Figure 5. PDOS of the oxygen-terminated surface for (a) GA2 and (b) GA2z. The Fermi energy is set to zero.

eV, with the Fermi level lying in the middle of the gap.[69] The valence band is dominated by oxygen atoms, specifically, oxygen p orbitals, which was observed in previous experimental and theoretical research.[2,28,69] Analyzing GA0z confirms the DOS that has the same overall structure (Figure 1b).

3.B. Surface Morphology (Slab Models). Upon slab creation, looking down at this surface, γ-Al_2O_3 has a visible hexagonal pattern among oxygen atoms, and we consider it to be a structural feature important to the surface stability and a factor in surface properties. When computing our various slab models, the bottom 40% of atoms of each slab was fixed at their optimized positions to imitate the bulk where atom movement occurs much more slowly and at much smaller distances than surface atoms.

γ-Al_2O_3 models' surface area for GA slabs is 31 Å^2 and for GAz slabs is 125 Å^2. The larger surface area is used to create a more realistic surface to account for noninteracting distortions.

3.B.i. Metal-Terminated Surface. Our theoretical model is the only one to date to study the γ-Al_2O_3 surface terminated with aluminum atoms, focusing on the electronic density of states for a dehydrated surface. Aluminum atoms can be exposed on the surface when dehydrated due to abnormalities within γ-Al_2O_3.[26,43] It might be expected that the Al-terminated γ-Al_2O_3 surface likely has high surface energy and low stability compared to the other surface models considered here. During the optimization of GA1, the surface underwent huge distortions on the surface. The most notable change was the vacancy increasing as the surface tetrahedral Al atom moved 1.8 Å toward the surface. This was a surprising result for this model, because in α-Al_2O_3, the most thermodynamically stable phase of Al_2O_3, all the cations are octahedrally coordinated and it does not have any vacancies. Thus, there is postulation that if there were any distortions of tetrahedral cations they would shift toward the vacancy, removing the defect. Instead, Al atoms moved toward the surface, with surface Al atoms becoming three-coordinated and in the same plane as oxygen atoms (Figure 2a). Such large atom movements upon surface optimization have been reported before for (110) and related to surface reconstruction, where the three-coordinated Al atoms drop from the surface layer into vacant octahedral interstices in the first subsurface layer.[24] The surface bond lengths between Al and oxygen are vastly larger than bulk bond lengths after surface optimization.

GA1z had very little surface atom rearrangements (Figure 2b). Surface Al atoms are three-coordinated with a small shift toward the vacuum, while the tetrahedral Al moved lower into the bulk. The bond lengths of surface Al−O atoms are shorter (between 1.7393 and 1.9540 Å) than those of GA1 (1.8957−2.1034 Å) but still longer than bulk Al−O bonds.

DOI: 10.1021/acs.jpcc.8b06506
J. Phys. Chem. C 2018, 122, 25314−25330

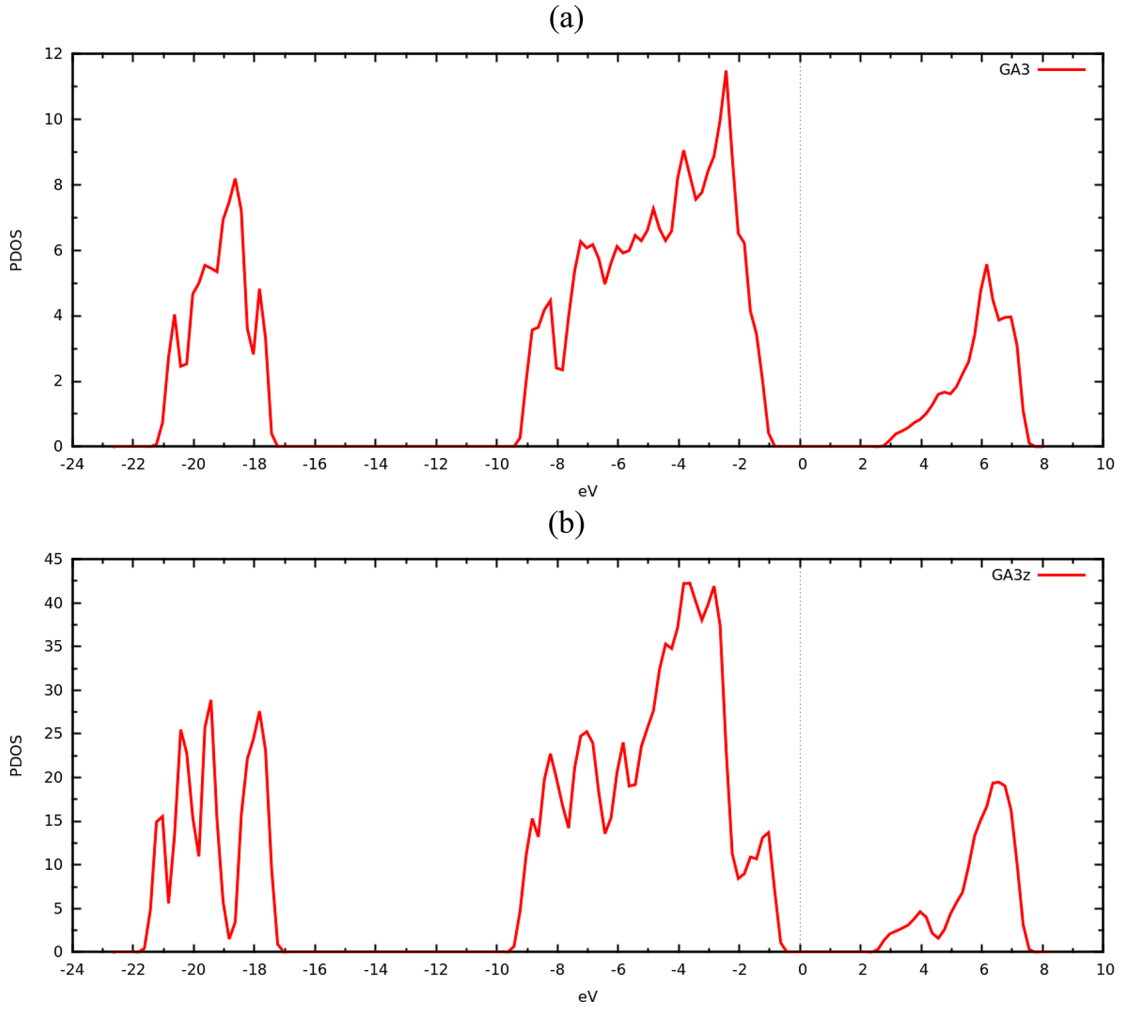

Figure 6. PDOS of the 100% hydroxylated surface of γ-Al_2O_3 for (a) GA3 and (b) GA3z. The Fermi energy is set to zero.

Table 2. Binding Energy (kcal/mol) of OH Removed from Various GA3/z (hydroxylated surface)[a]

removal site	GA3−OH[b]	GA3z−OH[c]
tetrahedral		
A	−144	−145
octahedral		
B	−145	−149
C	−147	−156
D	−159	−154

[a]See Figure 3 for a depiction of tetrahedral (A) and octahedral (B−D) sites. The negative sign signifies that work is needed to remove an OH group from these surface sites. [b]OH coverage of 0.097 OH/Å^2. [c]OH coverage of 0.12 OH/Å^2.

3.B.ii. Oxygen-Terminated γ-Al_2O_3. The second type of surface we model is an oxygen-terminated slab (GA2/z). The surface was created by cutting through the oxygen layer from bulk γ-Al_2O_3, and the slab was optimized. Optimization of the slab did not converge from its original surface structure. During the surface relaxation, one oxygen atom, located vertical to the tetrahedral Al, moved from this position to dimerize with one of the neighboring oxygens, which are bridged between two octahedral atoms. We believe this oxygen surface location to be an unstable site and was made vacant. This newly created surface (with the oxygen removed) was able to have the surface converge.

The GA2z slab underwent the same type of surface reconstruction with the oxygen atoms dimerizing from the tetrahedral location and then being removed to continue optimizing the surface. Upon optimization, surface atoms shifted, creating some five-coordinated aluminum atoms.

3.B.iii. 100% Hydroxylated γ-Al_2O_3 Surface. Lastly, we model a completely hydroxylated surface. The 100% hydroxylated surface of γ-Al_2O_3 (GA3/z) was constructed by the available sites from being cut at the oxygen layer in the bulk. The GA3 slab has a surface coverage of 0.13 OH/Å^2 with four hydroxyl groups with two types of coordination (Figure 3a). The first type of hydroxyl is only coordinated to one Al atom (tetrahedral site) and located vertical of it (hydroxyl A, Figure 3a). The second type of hydroxyl coordination is situated in the interstitial space, bridged between two octahedral Al atoms (hydroxyl B, Figure 3a). The GA3z slab has the same hydroxyl surface coverage with a total of 16 hydroxyls on the surface with four tetrahedral and 12 bridged hydroxyls (Figure 3b).

The optimized GA3 slab's reconstruction included hydroxyls having considerable rearrangement. The surface hydroxyls optimized to a network with the tetrahedral Al becoming four-coordinated and the hydroxyl group raising above the plane of the other surface hydroxyls (Figure 3c). Distortions among

DOI: 10.1021/acs.jpcc.8b06506
J. Phys. Chem. C 2018, 122, 25314−25330

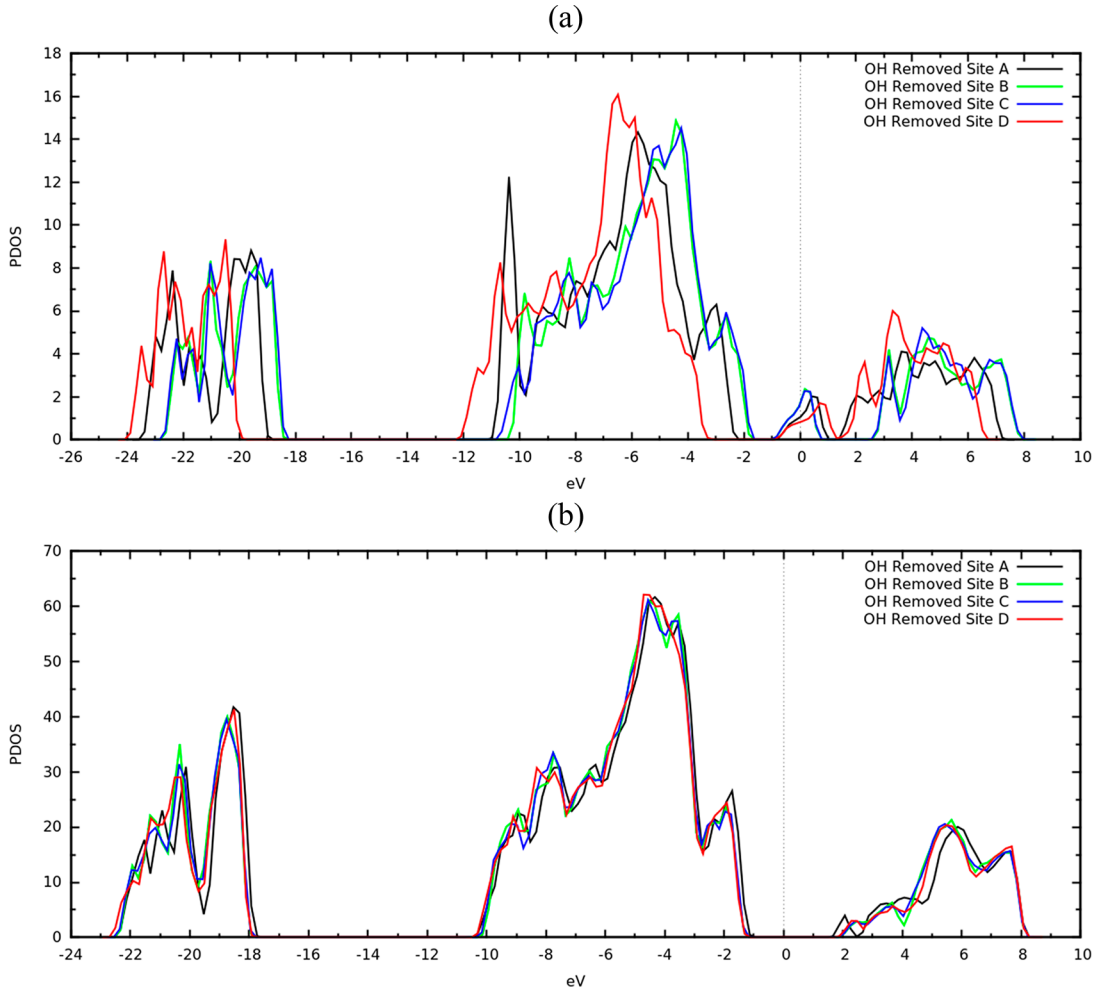

Figure 7. PDOS of OH removed from the surface for (a) GA3−OH and (b) GA3z−OH. The Fermi energy is set to zero.

Table 3. Binding Energy (in kcal/mol) of H_2O Removed from Fully Hydroxylated γ-Al_2O_3 Surface[a]

removal site	GA3−H_2O[b]	GA3z−H_2O[c]
tetrahedral		
A	−53	−50
octahedral		
B	−49	−51
C	−60	−46
D	−28	−69

[a]Two model structures are considered. A small, 40-atom model, GA3−H_2O, and a large 160-atom model, GA3z−H_2O. The negative sign signifies that work is needed to remove water from these surface sites. [b]OH coverage of 0.065 OH/Å^2. [c]OH coverage of 0.11 OH/Å^2.

subsurface aluminum atoms moved toward the bulk as much as 0.77 Å in GA3. The GA3z slab did not undergo dramatic surface reconstruction (Figure 3d). Hydroxyls have a more defined network and had less distortions among surface aluminum atoms moving a maximum of 0.28 Å toward the bulk.

3.C. Surface Electronic Properties of Metal, Oxygen, and Hydroxylated γ-Al_2O_3 Slabs. *3.C.i. Metal-Terminated Surface DOS.* The electronic properties of each surface display variations among the different optimized surface morphologies. The PDOS of the GA1 surface show a very small band gap of less than 1.0 eV (Figure 4a). The highest valence band peak occurs at −6.0 eV, attributed to oxygen p-orbitals. The PDOS plot does not represent a DOS plot reminiscent of an insulating material, where it should be in more in line with the DOS of bulk γ-Al_2O_3. To confirm these results, we analyzed GA1z, which has a different surface morphology than GA1, producing a dissimilar PDOS plot. The increased surface size displays the Fermi level within the conduction band. The Fermi level's current position (lying within the conduction band) results in a p-type characteristic material, therefore being noninsulating. The reduced band gap is the product of the increased surface states from the uncoordinated surface aluminum atoms. The extra states are attributed to the open/unsaturated sites and/or the dangling bonds of the aluminum surface cations, while negligible oxygen states also occur in the band gap.[69] Exposed surface ions have local acceptor states in the band gap, but they are accessible to gas-phase molecules and can act as Lewis acids with this exposed surface.[47,48,50,51,60] The dangling bonds as well as the increased surface strain might contribute to the catalytic activity of an adsorbent-free γ-Al_2O_3.

3.C.ii. Oxygen-Terminated Surface DOS. The electronic structure of the oxygen-terminated surface model differs compared to that of the metal-terminated (GA1/z) surface. The PDOS of the GA2 surface display a band gap of 3.0 eV. The surface states of the upper valence band are distributed between −8.0 and 1.0 eV and the conduction between 3.5 and 8.5 eV (Figure 5a). The Fermi level lies at the top of the

DOI: 10.1021/acs.jpcc.8b06506
J. Phys. Chem. C 2018, 122, 25314−25330

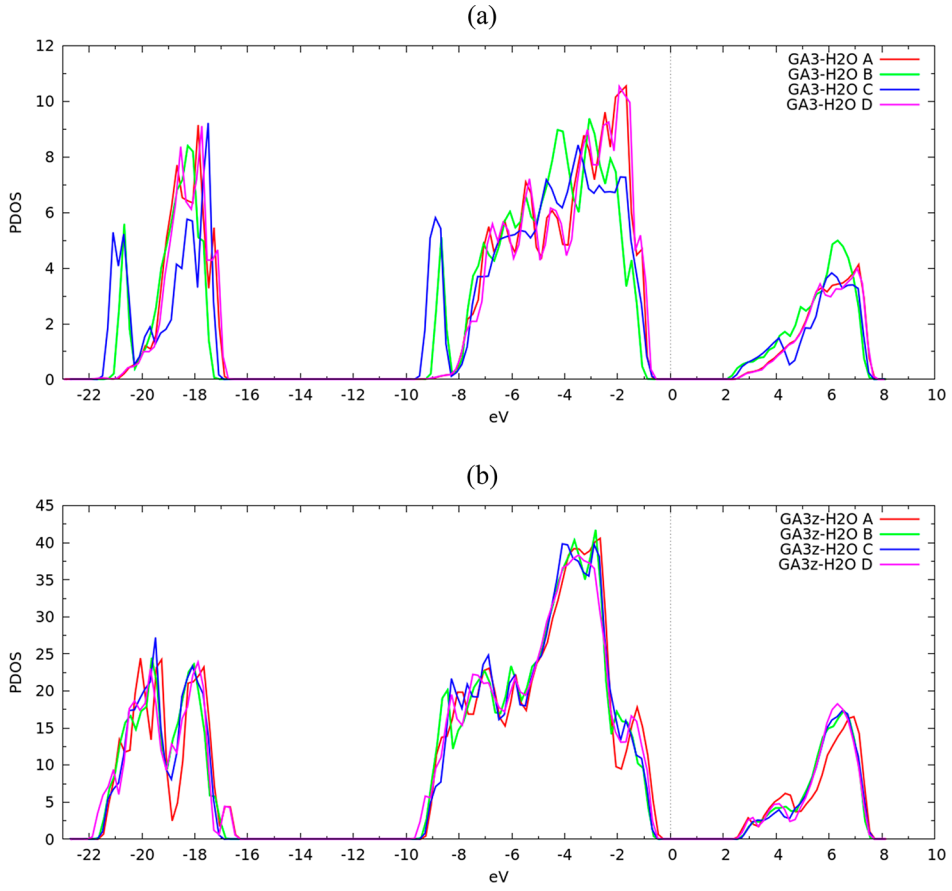

Figure 8. Calculated PDOS for when H_2O was removed from the γ-Al_2O_3 surface at different locations from (a) GA3−H_2O and (b) GA3z−H_2O. The Fermi energy is set to zero.

Table 4. Binding Energy (in kcal/mol) of H_2 Removed from GA3/z[a]

site	GA3−H_2[b]	GA3z−H_2[c]
1	−105	−113
2	−97	−115
3	−90	−102
4	−119	−114
5	n/a	−104
6	n/a	−98
7	n/a	−112

[a]n/a means no site available to calculate. The negative sign signifies that work is needed to remove molecular hydrogen from these surface sites. [b]OH coverage of 0.065 OH/Å^2. [c]OH coverage of 0.11 OH/Å^2.

valence band, which also features most states occurring at this energy level. Once again, the valence band, as shown in previous studies, is associated with the oxygen (s and p) orbitals, with the p-orbitals dominating.[3,7,31] GA2/z slabs have states occurring at the top of the valence band that did not evolve in GA1/z. The shapes of the GA2/GA2z valence and conduction bands are different between the aluminum-terminated and oxygen-terminated slabs. The oxygen-terminated surface shows oxygen atoms occupying the dangling bonds manifested in GA1/z.

3.C.iii. Hydroxylated Surface DOS. The computed PDOS of GA3 display a distinct band gap of 3.8 eV, only slightly smaller than the calculated band gap of bulk γ-Al_2O_3. The Fermi level for the GA3 was also calculated near the top of the valence band, thus showing that the Fermi level is not completely dependent on surface hydroxylation. Analysis of GA3z, which has a slightly different surface structure, confirms this electronic structure (Figure 6b). There are noticeable differences between the two surface sizes at the top of the valence band and the bottom of the conduction band. At both sites an extra peak occurs, indicating a clear shift in the surface atoms' energy states.

3.D. Elimination of Adsorbents from the Hydroxylated γ-Al_2O_3 Surface. The use of γ-Al_2O_3 in industry is usually done at high temperatures, which lead to the elimination of adsorbents from the surface. We model the elimination of OH, H_2O, and H_2. This will give insight into the binding energy of the species and how the surface changes as adsorbents are removed from the surface. The set of binding energies allows us to understand the overall reactivity of the surface; i.e., the sites featuring the lowest binding energy will be more prone to chemical reactivity than the other sites.

3.D.i. Removal of OH. Specifically, we removed one hydroxyl from the GA3 slab out of the four hydroxyls at each location, leaving the surface coverage 0.096 OH/Å^2. The binding energy (BE) of the hydroxyls was calculated by

$$E_{\mathrm{BEOH}} = E_{\gamma\text{-}Al_2O_3-\mathrm{OH}} + E_{\mathrm{single\,OH}} - E_{\gamma\text{-}Al_2O_3+\mathrm{OH}} \quad (1)$$

The surfaces for these models do not maintain a stoichiometric unit cell if interpreting the removal of OH as a hydroxide rather than a radical specie. Three of the OHs had different energies, with the lowest BE of 140 kcal/mol being from the hydroxyl located vertical to the tetrahedral aluminum atom,

DOI: 10.1021/acs.jpcc.8b06506
J. Phys. Chem. C 2018, 122, 25314−25330

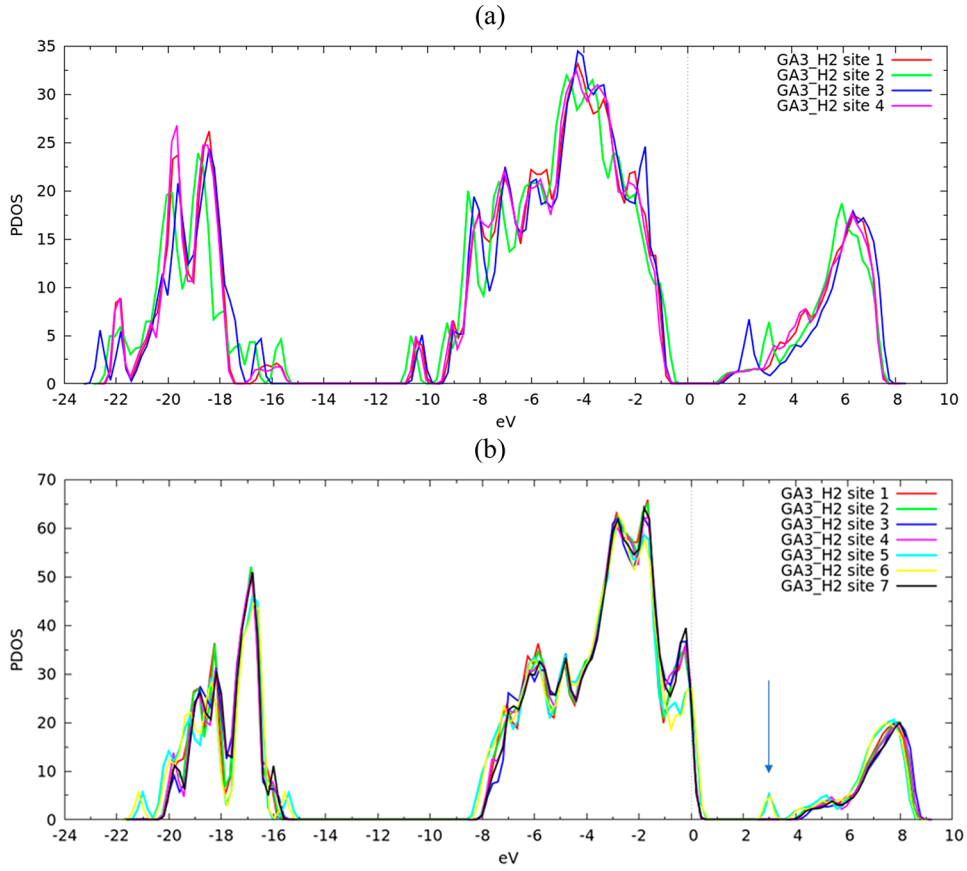

Figure 9. PDOS of H_2 removed at various locations on (a) GA3−H_2 and (b) GA3z−H_2. The Fermi energy is set to zero.

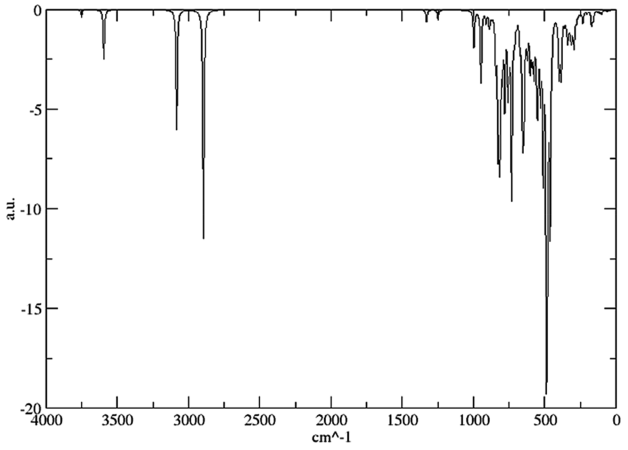

Figure 10. Calculated vibrational frequency of the hydrated small-cell slab (GA3).

hydroxyl A (Figure 3, Table 2). Removal of the hydroxyl left the aluminum atom to sink toward the bulk to become four-coordinated (Figure S6, SI). The optimized surface included distortions, with the hydroxyls arranging on the surface to point toward the vacancy, toward each other, causing an increase in hydrogen−hydrogen repulsion. This is due to the small surface area where neighboring unit cells influence the hydroxyl arrangement in an undesirable, high energy surface.

The second type of hydroxyl on the surface removed is situated in the interstitial space, bridged between two octahedral Al atoms (hydroxyl B, C, and D). This resulted in substantial surface distortions as well, which included surface atoms moving toward the vacuum. Surface Al atoms encompassed four- and five-coordinated oxygen. When each of the three bridged hydroxyls were removed, being optimized with different surface configuration. However, the BE was calculated to be the same at each position at 131 kcal/mol.

When analyzing the removal of OH from GA3z's 16 surface hydroxyls, of them, 4 OH removed had different BE (denoted as GA3z−OH). The hydroxyl with the lowest BE was not at the same site as GA3 but at an octahedral, bridged, site. The hydroxyl surface coverage after OH removal is 0.12 OH/Å^2, which is higher than that of GA3−OH (Figure 3, Table 2). The surface did not undergo any substantial rearrangements (Figure S7, SI). This can be attributed to the increased surface area or the higher hydroxyl surface concentration helping to stabilize the surface. Various bridged hydroxyls removed from GA3z optimizations entailed three, four, and five aluminum atoms that have been experimentally observed.[17,64] Hydroxyl C on GA3z had the least amount of surface rearrangements during optimization, resulting in the lowest BE of 156 kcal/mol. This hydroxyl site had the greatest distortions. Our results are in accordance with the previous result[71] for the adsorption energy of OH reported for (001), (011), and (111) planes of γ-Al_2O_3. It was reported that under fully relaxed surfaces the value changes between 7.8 and 11.3 eV (179.9 and 260.6 kcal/mol), while under ideal (unrelaxed) surfaces it changes between 2.6 and 12.6 (60.0 and 290.6 kcal/mol).

Electronic Structure of OH-Removed Surface Models. The PDOS were calculated for each hydroxyl removed from GA3 and GA3z surfaces. The differing energies of the hydroxyls BE and OH coverage coordinated with the different surface state structures. The PDOS of GA3−OH removal generated

DOI: 10.1021/acs.jpcc.8b06506
J. Phys. Chem. C 2018, 122, 25314−25330

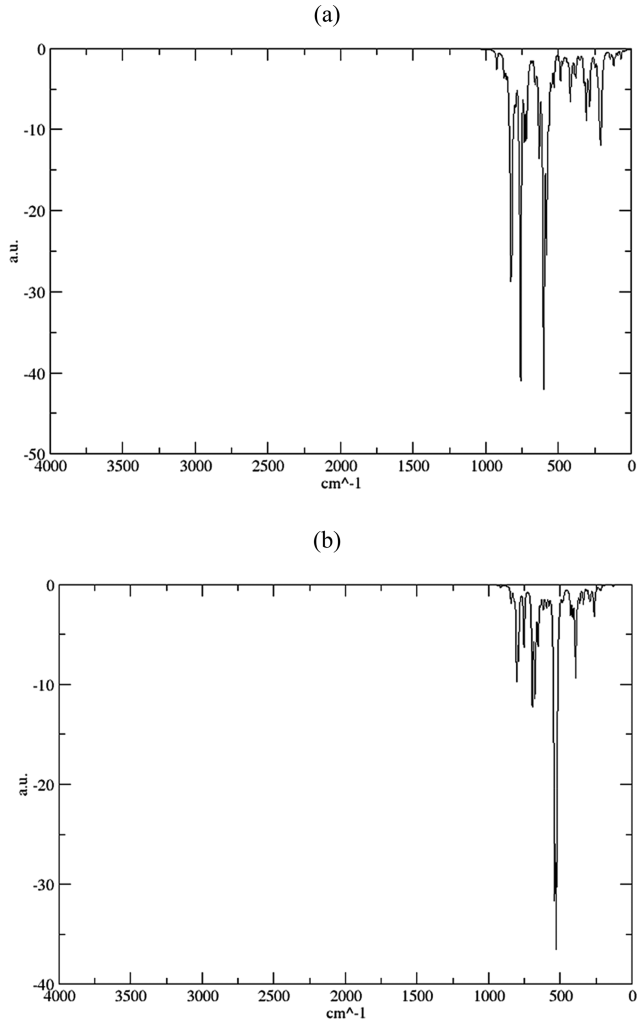

Figure 11. Vibrational frequency of the (a) oxygen-terminated surface (GA2) and (b) bulk γ-Al_2O_3 (GA0).

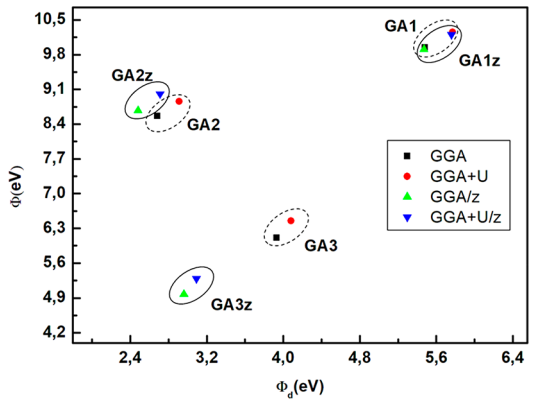

Figure 12. Plot of the work function (ϕ) vs the surface dipole contribution (ϕ_d).

dissimilar states at each removal site, as shown in Figure 7a. The GA3−OH has the Fermi level in the band gap of 4.0 eV. In addition, surface states emerge within the band gap. These states occur from the optimized tetrahedral Al atom that is three-coordinated upon OH removal. There is a clear shift in the Fermi energy for hydroxyl D, which is the site with the largest distortions and BE. The larger surface area and higher OH concentration of GA3z−OH PDOS did not generate the same band gap surface states (Figure 7b). This shows the importance of sizable finite size effects and that surface relaxation effects must be taken into account when modeling γ-Al_2O_3 surfaces. The PDOS show a smaller band gap of 3.0 eV with the Fermi level centered in the gap. The plot displays a nearly identical DOS between each OH removal site with subtle differences in the conduction band.

3.D.ii. Removal of H_2O. The removal of OH from the γ-Al_2O_3 surface is a possible mechanism, but entails a higher-order reaction.[44] It was reported that when the surface is heated water is expelled from the surface as the temperature increases.[66] We model this process and calculated the BE of water at various locations. We believe H_2O will be eliminated first from the tetrahedral Al site; this site had the lowest OH BE. The mechanism of H_2O elimination would occur with the tetrahedral hydroxyl and bind to its nearest neighboring hydrogen atom (see the SI, Figure S4 for GA3−H_2O and Figure S5 for GA3z−H_2O structures). The nearest hydrogens in GA3 and GA3z are 1.59 Å away from the tetrahedral hydroxyl. The BE of water was calculated by

$$E_{\mathrm{BEH_2O}} = E_{\gamma\text{-}\mathrm{Al_2O_3}-\mathrm{H_2O}} + E_{\mathrm{single\,H_2O}} - E_{\gamma\text{-}\mathrm{Al_2O_3}+\mathrm{H_2O}} \quad (2)$$

Removing water from GA3 (referred to as GA3−H_2O) causes the surface to have a hydroxyl coverage of 0.065 OH/Å^2. The calculated BE of water removed from the tetrahedral Al site (hydroxyl A from Figure 3a) has a value of −53 kcal/mol. The surface optimized to have the tetrahedral Al atom move toward the surface stays three-coordinated. Water removed from the same location for GA3z (referred to GA3z−H_2O) has a BE of −50 kcal/mol. A small energy change can be attributed to the higher hydroxyl coverage of 0.11 OH/Å^2.

Then water removal from octahedral/bridged sites was modeled to verify if location influences the binding energy. The BE of water at each octahedral site can be found in Table 3. Among GA3−H_2O surface removal sites, the BE changes drastically between each site, representing the different surface morphologies upon optimization. When water was removed with hydroxyl B and it nearest neighboring hydrogen atom, the surface optimized to have an H_2O molecule on the tetrahedral aluminum atom (see Figure S4, SI). For water removal with hydroxyl C, the tetrahedral aluminum atom sunk toward the bulk, becoming five-coordinated. The last possible water removal site using hydroxyl D ended with the smallest BE, which infers a relatively higher strained surface.

For GA3z, we calculated three different BE values for H_2O removed at octahedral surface locations (sites B, C, and D), as seen in Table 3. The water removed at site B (GA3z−H_2O) and site C had close BEs, showing similar atomic surface reorganization, shifting hydrogen molecules across the surface. However, site C had a lower BE than site A and was more likely to be eliminated first. Site C also had H_2O temporarily formed on the tetrahedral Al site; however, this optimized surface configuration caused two H−O bonds to be broken and re-formed. The last water removal location, site D, had the least hydroxyl reconstruction but the largest BE, which can be attributed to the aluminum atom distorting to bind with a subsurface oxygen atom. So far, our models affirm that water will be eliminated from the surface first, leaving the surface more stable than elimination of hydroxyl species.

Our calculated BE energy of H_2O on our γ-Al_2O_3 models are comparable to adsorption and/or desorption energies of water from former experimental studies and theoretical calculations.

DOI: 10.1021/acs.jpcc.8b06506
J. Phys. Chem. C 2018, 122, 25314−25330

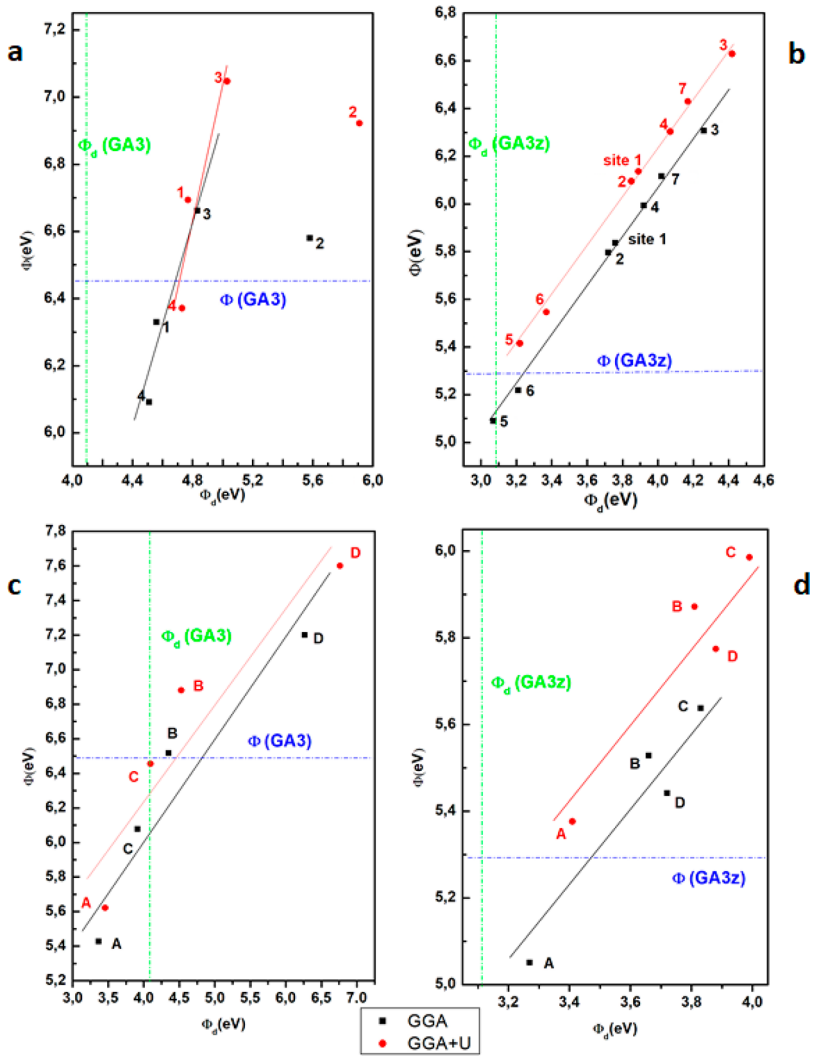

Figure 13. Plot of work function (ϕ) vs surface dipole contribution (ϕ_d) for the treatment on GA3/GA3z models: (a) GA3−H_2, (b) GA3z−H_2, (c) GA3−H_2O, and (d) GA3z−H_2O. The solid red/black lines are used to show the linear behavior. The indicated ϕ (horizontal dashed line) and ϕ_d (vertical dashed line) are the values of GA3 and GA3z calculated by GGA+*U*.

H_2O on γ-Al_2O_3 and/or other metal oxides at various OH surface coverage and *hkl* surfaces have been computed by Zamora and Cordoba,[38] Fleisher et al.,[48,72] Ionescu et al.,[42] and Digne et al.[11,46] They calculated the desorption energy of water on the (111) surface of γ-Al_2O_3 to be 37 and 46 kcal/mol, associated with 10.0 and 3.0 OH/nm^2 surface coverage, respectively.[46] On the (100) and (110) surfaces the desorption energy of water was between 16 and 21 kcal/mol.[7] The adsorption energy of water was also theoretically studied on a variety of *hkl* surfaces at different hydroxyl coverages, ranging from 16 to 65 kcal/mol for the (110), (111), and (100) surfaces.[20,34,36,41,73−75] In each study, the adsorption energy changed, depending on OH surface coverage determined by the associated temperature.

Other theoretical studies on the adsorption of water were done on isolated octahedral and tetrahedral Al atoms. The adsorption energies on the octahedral Al were 19 and 29 kcal/mol and on tetrahedral Al were 56 and 60 kcal/mol.[76] Experimental research on the adsorption of water at these two locations had an energy of 26 kcal/mol at the octahedral Al atom and 45 kcal/mol on the tetrahedral Al.[47,75,76] Our computed BEs from the (001) γ-Al_2O_3 model surface, for both the small cells and supercells at the tetrahedral site, achieve similar energies to previously reported adsorption and/or desorption energies of water.

DOS of H_2O Removal. The PDOS of GA3−H_2O at different sites reveal the small differences associated with the different locations where water is removed. The calculated band gap is about 2.5 eV, with the Fermi level lying at the top of the valence band (Figure 8a). In contrast, GA3z−H_2O has a band gap of 3.0 eV and nearly identical PDOS between each site (Figure 8b). The higher OH surface concentration did not induce large surface changes. These changes usually do not arise until more water is eliminated from the surface.

3.D.iii. Removal of H_2. The last type of molecule removed from our surface model was H_2. This was done at a variety of locations, leaving the OH coverage to be 0.065 OH/Å^2. GA3−H_2 had distortions occur among the surface oxygen atoms to form oxygen dimers. The BE for H_2 was calculated by

$$E_{\mathrm{BEH_2}} = E_{\gamma\text{-}\mathrm{Al_2O_3}-\mathrm{H_2}} + E_{\mathrm{H_2}} - E_{\gamma\text{-}\mathrm{Al_2O_3}} \quad (3)$$

The calculated BE of H_2 for GA3−H_2 was between −90 and −119 kcal/mol (Table 4). The formation of dimers occurred when H_2 was removed from the tetrahedral Al site. The

DOI: 10.1021/acs.jpcc.8b06506
J. Phys. Chem. C 2018, 122, 25314−25330

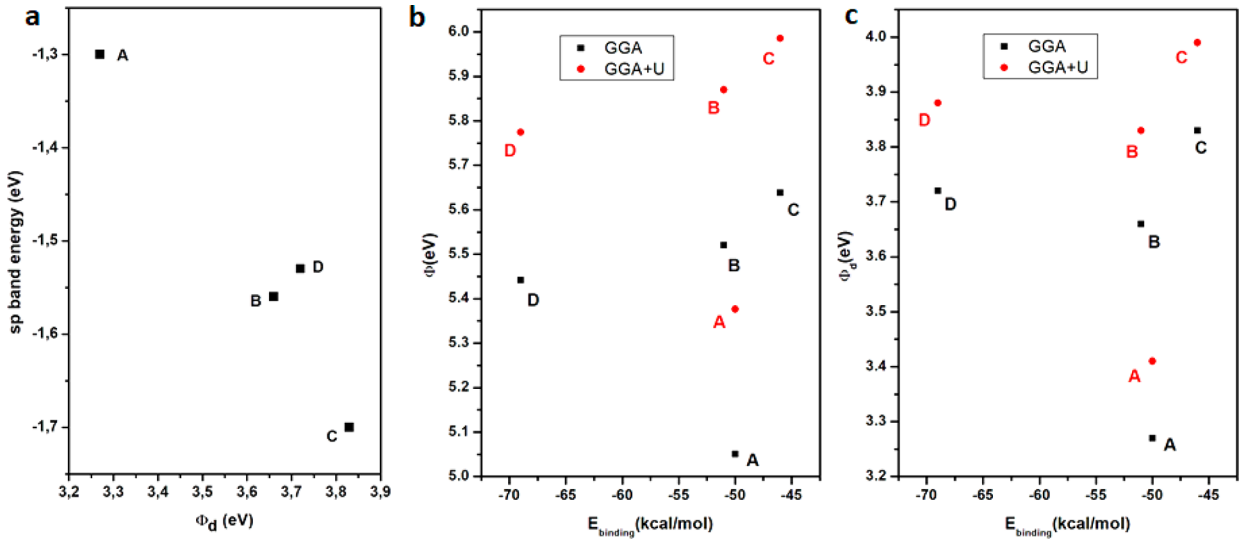

Figure 14. Plot of (a) the PDOS on 3s and 3p orbitals of surface Al atom vs surface dipole contribution (ϕ_d), (b) work function (ϕ) vs binding energy ($E_{binding}$), and (c) surface dipole contribution (ϕ_d) vs binding energy ($E_{binding}$) for GA3z−H_2O surface models. The correlation in the plot occurs for the octahedral Al atoms (B, C, and D). In our models, we only have one tetrahedral Al atom and thus could not inspect the correlation for tetrahedral Al atoms.

decreased BE for sites 2 and 3 is associated with the formation of an oxygen dimer on the surface as well as a water molecule configuration. The higher OH coverage of GA3z−H_2 at 0.11 OH/Å has little effect on the BE of H_2, which ranged between −98 and −115 kcal/mol (Table 4). Water remains to have the lowest BE and therefore would most likely to be eliminated from the surface when heated.

DOS of H_2 Removed from the γ-Al_2O_3 Surface. The PDOS structures for all H_2 removal sites from GA3 are very similar to a band gap of 3.5 eV (Figure 9a). The Fermi level was calculated to be at the top of the valence band. New peaks at 2.5 eV from site 3 and at 3.0 eV from site 2 are associated with the formation of oxygen dimer. The electronic structures of GA3z−H_2 once again have nearly identical plots, with the Fermi level at the top of the valence band. However, the surface morphology where an oxygen dimer forms gives rise to surface states in the band gap (Figure 9b).

3.E. Surface Energies. The relative surface energy of GA1/z (metal-terminated) was calculated and compared to a variety of *hkl* surfaces from previous research. To have a more consistent bulk value to calculate the surface energy, we interpolated the energy of varying the total number of atoms for γ-Al_2O_3.[7,77] The slope of the line is the bulk energy used for *N* number of atoms. Our GA1 slab has a surface energy of 1.93 J/m^2 and GA1z one of 2.01 J/m^2. Our values are slightly higher in energy than the reported surface energy values of the (001) surface from Pinto et al.[7] (1.05 J/m^2 for the relaxed surface and 2.97 J/m^2 for the static surface). Other reported γ-Al_2O_3 surface energies from optimized, static, and experimental γ-Al_2O_3 ranged between 0.9 and 4.0 J/mol.[3,7,78,79] The surface energies we calculated are comparable to earlier calculated energies, but differences arise from the type of *hkl* surface and/or surface termination calculated.[7,77,80] Importantly, this is contrary to the aforementioned expectation of the Al-terminated γ-Al_2O_3 surface having relatively high surface energy and low stability.

3.F. IR Spectra. Surface details provided by vibrational spectroscopy experiments produced IR spectra with peaks attributed to at least five different surface hydroxyl groups.[42,43,78,81] These emerge due to the specific surface sites and the surrounding environment, and can be described to being one-, two-, and/or three-coordinated OH groups to Al atoms.[60] Analysis of hydroxyls on our γ-Al_2O_3 surfaces included calculating the vibrational frequencies for the GA3, GA2, and GA0. The GA3 surface, as explained before, has two types of hydroxyl coordination, one- and two-coordinated OH to surface Al atoms. Vibrational frequencies of the hydrated surface showed four maximum peaks between 2750 and 4000 cm^{-1} (Figure 10). The four peaks are associated with the different hydroxyls on the surface. Peri and Hannan[81] reported wave numbers for different hydroxyls between 3800 and 3200 cm^{-1} based on the number of nearest oxide neighbors.[43] Other studies also reported higher vibrational frequencies for hydroxyl groups, with the lowest frequency around 3500 cm^{-1}.[4,11,46,60,68] Al-Abadleh and Grassian[34] showed that at low OH coverage the OH absorption maximum was 3444 cm^{-1} with a stretching region at 3188 and 3583 cm^{-1} and at high water coverage an absorption at 3381 cm^{-1}. One unexplained IR spectrum feature from a previous report was a band occurring around ∼2800 cm^{-1}. We show that this intense IR peak exists on our surface, which is associated with one of the bridged hydroxyls undergoing hydrogen bonding and can also be seen in the FTIR spectrum of Costa et al.[5] Hydrogen bonding lowers the OH vibrational frequency. The tetrahedral OH is responsible for the peak around 3750 cm^{-1}, while the bridged OH groups absorb a much lower IR frequency, in the window of 3000−3600 cm^{-1}. The high-energy modes are consistent (within 50 cm^{-1} difference) with the unassigned frequencies from experimental spectra of γ-Al_2O_3.[4,11,36]

The vibrational frequencies were also calculated for bulk (GA0) and oxygen-terminated (GA2) γ-Al_2O_3 surfaces, which obviously do not show any sign of hydroxyl groups (Figure 11). All spectra display the fingerprint region between 250 and 1000 cm^{-1}. The GA2 also shows strong peaks at 750 and 800 cm^{-1}, while medium to medium−weak peaks for GA0 and GA3 are seen at the same wavenumber. The IR spectrum in this range aligns with tetrahedral and octahedral Al−O

DOI: 10.1021/acs.jpcc.8b06506
J. Phys. Chem. C 2018, 122, 25314−25330

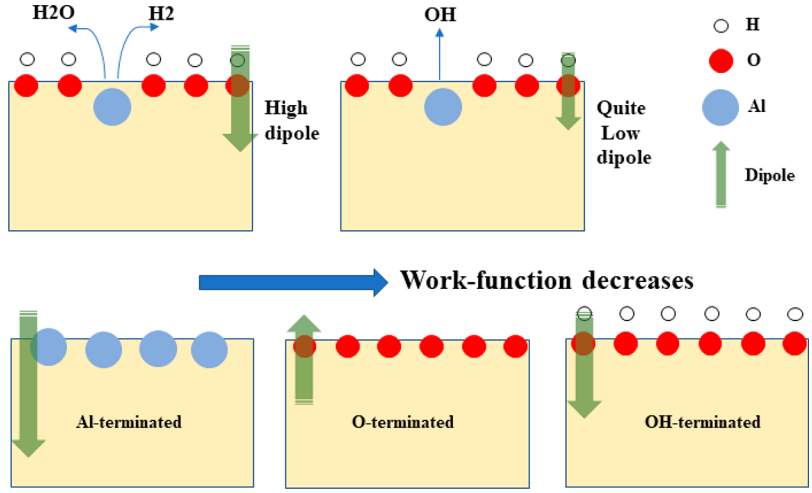

Figure 15. Surface–function correlation between the electronic properties and morphology.

frequencies that are comparable to previous experimental studies.[53,66,82]

3.G. Work Functions and Surface Dipoles. The work function (WF, ϕ) has a particular role in catalysis because it is an important surface electronic structure property. Thus, it has been usually investigated to better understand the performance of catalyts. Recently, the changes of WF with film thickness on γ-Al_2O_3 thin film samples were explored.[83] A slight change of WF, from 4.1(6) to 3.9(3) eV, was obtained with increasing the film thickness, from 0.4 to 1.5 nm. In addition to our previous calculations, so as to further trace the effect of the various topological possibilities on the surfaces as well as to get a structure–function relationship in terms of correlation between the WF and the binding energy, we have computed the variation of the work function, which can strongly estimate the behavior of the electronic structure against the various surface formations.

We have carried out DFT calculations for all γ-Al_2O_3 surface models for which the codes were developed in the Quantum-ESPRESSO package version 6.1. In these calculations, in addition to the normal DFT (GGA) computations, we also employed a GGA+U method of calculation for the WFs of all surface models. In performing GGA+U, we utilized a suitable U value for O (1.11 eV) that we derived by employing the Cococcioni–de Gironcoli linear response method[84] to the small surface structures (40 atoms). In addition to the WF, we also computed the size of the surface dipole contribution to ϕ (denoted as ϕ_d), which was estimated by computing the difference between the left and right vacuum levels. These can be seen for each model under study in the plane-averaged electrostatic potential plots (Figures S8–S34, SI). Furthermore, the numerical values of all calculated ϕ and ϕ_d are tabulated in Table S1 (SI).

A comparison of the small-cell structures (GA) with the supercell ones (GAz) for the basic structures is depicted in Figure 12. Upon inspecting this figure and the results in Table S1 (SI), we see that in general both the WF and surface dipole contribution (ϕ_d) of GA3z models are found to be less than the GA3 ones. This shows that size and morphology are two main factors strongly affecting WF and dipole. The results of GA1 and GA1z surface models indicate that the metal termination (dehydrated) induces very high ϕ and ϕ_d. It is seen that the most profound treatment is OH-removal on GA3/GA3z models, which drastically changes both WF and ϕ_d on OH-terminated surfaces (GA3–OH/GA3z–OH). Also, the calculated quantities using GGA+U are all consistent and a bit higher compared to those calculated with GGA.

To reach a correlation between the WF and surface dipole contribution for all the H_2 and H_2O treatments on GA3/z models, we plot ϕ–ϕ_d as shown in Figure 13. It is clearly seen that all these treatments result in higher ϕ_d on the basic models GA3/z. In general, GA3 models appear better linearly correlated with regard to the ϕ–ϕ_d relation. Figure 13 shows that there exists almost a linear correlation between ϕ and ϕ_d for the models of these treatments, especially for GA3z–H_2 (Figure 13b) and GA3–H_2O (Figure 13c). In GA3–H_2 (Figure 13a), we see that site 2 does not obey the linearity. This may be due to formation of an oxygen dimer on the surface of this site and/or a water molecule configuration, as mentioned before (see Figure S1, SI). It is also seen that less correlation for ϕ–ϕ_d occurs for GA3z–H_2O, which may come from the unfavorable larger surface rearrangement in these models mentioned before (see Figure S5, SI).

In order to understand the effect of surface properties (such as the dipole moment) on the chemical behavior of γ-Al_2O_3 and its specific active sites, we embarked on an analysis of the electronic structure of uncoordinated Al surface sites that result from a dehydration. Figure 14a shows a clear correlation between the surface dipole ϕ_d and the PDOS peak given by the Al 3s–3p band of the Al dehydration site (from the GA3z–H_2O surface models). This is an important observation, because it indicates that the energy levels of the active Al sites are affected by the surface dipole. This, in turn, will modify their alignment with energy levels of other species. This is a typical case of a nonadditive, synergistic effect, where the chemical properties of a specie vary in relation to other, global properties of the system. This is confirmed by Figure 14b,c, where the binding energy of water on the surface is clearly correlated to the surface dipole.

The work function vs dipole plot that we presented previously (i.e., ϕ vs ϕ_d plot of Figure 13d) follows the same trend as the binding energies and 3sp band energies. Thus, we can speculate that the surface dipole moment is an important descriptor that correlates to an array of chemical and physical properties of γ-Al_2O_3.

DOI: 10.1021/acs.jpcc.8b06506
J. Phys. Chem. C 2018, 122, 25314–25330

4. CONCLUSION

We performed semilocal DFT and DFT+U simulations of model surfaces of γ-Al_2O_3. We computed electronic density of states; binding energy of H_2O, H_2, and OH groups; and surface work functions. Our simulations show that there are two important factors that need to be taken into account when studying surface electronic properties: surface coverage and the specific local environment surrounding the site of interest. We find that the stability of surface groups and electrostatic properties of the surface (such as work function and surface dipole) are correlated.

We also computed surface energies associated with our model structures. We find that they are comparable to those that have been previously reported, thus indicating that our model structures are plausible. Our model indicates that hydroxyls can be found bridged between octahedral and tetrahedral aluminum atoms and between octahedral aluminum atoms depending on the degree of water elimination. This is in agreement with the work of Liu and Truitt[68] that showed experimental data of hydroxyls reaching high coordination. We suggest that, with an open coordination site, the hydroxyl will be able to migrate to a place to coordinate.

The structure−function correlation between the electronic properties and morphology has been probed for γ-Al_2O_3 surfaces. Our simulations reveal a trend in the work function when comparing different surface terminations. Namely, the surfaces terminated by metals or oxygens feature the highest work function. Our explanation for the low work functions of hydroxylated surfaces rests on the electrostatic properties of the surfaces. The OH groups provide a dipole moment that is strong and opposite to the one of the nonhydroxylated surfaces. We summarize this overarching concept in Figure 15.

We find that the electronic DOS, binding energy, and work function of OH-, H_2O-, and H_2-abstracted hydroxylated γ-Al_2O_3 models depend strongly on the desorption site. Correlation of the binding energy of these species with the work function and surface dipole demonstrates that a nonadditive/synergistic effect for water adsorption is present, for which the surface dipole moment is a driving force.

ASSOCIATED CONTENT

Supporting Information

The Supporting Information is available free of charge on the ACS Publications website at DOI: 10.1021/acs.jpcc.8b06506.

Collection of input files of all models considered (Figures S1−S34 and Table S1) (PDF)

AUTHOR INFORMATION

Corresponding Authors

*M.A. e-mail: muhammed.acikgoz@rutgers.edu.
*M.P. e-mail: m.pavanello@rutgers.edu.

ORCID

Muhammed Acikgoz: 0000-0003-4165-0854
Michele Pavanello: 0000-0001-8294-7481

Author Contributions

†M.A. and J.H. contributed equally to this work.

Notes

The authors declare no competing financial interest.

ACKNOWLEDGMENTS

This material is based upon work supported by the National Science Foundation under Grant number DMR-1742807. We thank Dr. Alessandro Genova for helping setting up the work function calculations and input files.

REFERENCES

(1) Kefi, M.; Jonnard, P.; Vergand, F.; Bonnelle, C.; Gillet, E. Hybridization of Al and O States in α-Alumina and γ-Alumina. *J. Phys.: Condens. Matter* **1993**, *5*, 8629−8642.

(2) Gutiérrez, G.; Taga, A.; Johansson, B. Theoretical structure determination of γ-Al_2O_3. *Phys. Rev. B: Condens. Matter Mater. Phys.* **2001**, *65*, 012101.

(3) Ouyang, C.; Šljivančanin, Ž.; Baldereschi, A. First-principles study of γ-Al_2O_3 (100) surface. *Phys. Rev. B: Condens. Matter Mater. Phys.* **2009**, *79*, 235410.

(4) Morterra, C.; Magnacca, G. A case study: Surface chemistry and surface structure of catalytic aluminas, as studied by vibrational spectroscopy of adsorbed species. *Catal. Today* **1996**, *27*, 497−532. Santos, P. S.; Santos, H. S.; Toledo, S. P. Standard transition aluminas: electron microscopy studies. *Mater. Res.* **2000**, *3*, 104−114.

(5) Costa, T. M. H.; Gallas, M. R.; Benvenutti, E. V.; da Jornada, J. A. H. Study of nanocrystalline γ-Al_2O_3 produced by high-pressure compaction. *J. Phys. Chem. B* **1999**, *103*, 4278−4284.

(6) Paglia, G.; Buckley, C.; Rohl, A.; Hunter, B.; Hart, R.; Hanna, J.; Byrne, L. Tetragonal structure model for boehmite-derived γ-alumina. *Phys. Rev. B: Condens. Matter Mater. Phys.* **2003**, *68*, 144110. Schuit, G. C.; Gates, B. C. Chemistry and engineering of catalytic hydrodesulfurization. *AIChE J.* **1973**, *19*, 417−438.

(7) Pinto, H. P.; Nieminen, R. M.; Elliott, S. D. Ab initio study of γ-Al_2O_3 surfaces. *Phys. Rev. B: Condens. Matter Mater. Phys.* **2004**, *70*, 125402.

(8) Trueba, M.; Trasatti, S. P. γ-Alumina as a support for catalysts: A review of fundamental aspects. *Eur. J. Inorg. Chem.* **2005**, *2005*, 3393−3403.

(9) Li, J.; Zhang, R.; Wang, B. Influence of the hydroxylation of γ-Al2O3 surfaces on the stability and growth of Cu for Cu/γ-Al2O3 catalyst: A DFT study. *Appl. Surf. Sci.* **2013**, *270*, 728−736.

(10) Barr, T. L.; Seal, S.; Chen, L. M.; Kao, C. C. A new interpretation of the binding energies in X-ray photoelectron studies of oxides. *Thin Solid Films* **1994**, *253*, 277−284.

(11) Digne, M.; Sautet, P.; Raybaud, P.; Euzen, P.; Toulhoat, H. Hydroxyl groups on γ-alumina surfaces: A DFT study. *J. Catal.* **2002**, *211*, 1−5.

(12) Valero, M. C.; Raybaud, P.; Sautet, P. Interplay between molecular adsorption and metal-support interaction for small supported metal clusters: CO and C2H4 adsorption on Pd-4/gamma-Al2O3. *J. Catal.* **2007**, *247*, 339−355.

(13) Wilson, S. J. The dehydration of boehmite, γ-AlOOH, to γ-Al2O3. *J. Solid State Chem.* **1979**, *30*, 247−255.

(14) Kasprzyk-Hordern, B. Chemistry of alumina, reactions in aqueous solution and its application in water treatment. *Adv. Colloid Interface Sci.* **2004**, *110*, 19−48.

(15) Vijay, A.; Mills, G.; Metiu, H. Structure of the (001) surface of gamma alumina. *J. Chem. Phys.* **2002**, *117*, 4509−4516.

(16) Paglia, G.; Bozin, E. S.; Billinge, S. J. L. Fine-scale nanostructure in gamma-Al2O3. *Chem. Mater.* **2006**, *18*, 3242−3248.

(17) Paglia, G.; Rohl, A. L.; Buckley, C. E.; Gale, J. D. Determination of the structure of γ-alumina from interatomic potential and first-principles calculations: The requirement of significant numbers of nonspinel positions to achieve an accurate structural model. *Phys. Rev. B: Condens. Matter Mater. Phys.* **2005**, *71*, 224115.

(18) Wolverton, C.; Hass, K. Phase stability and structure of spinel-based transition aluminas. *Phys. Rev. B: Condens. Matter Mater. Phys.* **2001**, *63*, 024102.

(19) Sohlberg, K.; Pennycook, S. J.; Pantelides, S. T. Hydrogen and the structure of the transition aluminas. *J. Am. Chem. Soc.* **1999**, *121*, 7493−7499.

DOI: 10.1021/acs.jpcc.8b06506
J. Phys. Chem. C 2018, 122, 25314−25330

(20) Paglia, G.; Buckley, C. E.; Udovic, T. J.; Rohl, A. L.; Jones, F.; Maitland, C. F.; Connolly, J. Boehmite-derived gamma-alumina system. 2. Consideration of hydrogen and surface effects. *Chem. Mater.* **2004**, *16*, 1914−1923.
(21) Wefers, K.; Misra, C. *Oxides and Hydroxides of Aluminum*; ALCOA Research Laboratories: Pittsburgh, PA, 1987; Technical Paper No. 19.
(22) Zhou, R. S.; Snyder, R. L. Structures and Transformation Mechanisms of the Eta, Gamma and Theta Transition Aluminas. *Acta Crystallogr., Sect. B: Struct. Sci.* **1991**, *47*, 617−630.
(23) Sohlberg, K.; Pennycook, S. J.; Pantelides, S. T. The bulk and surface structure of gamma- alumina. *Chem. Eng. Commun.* **2000**, *181*, 107−135.
(24) Sohlberg, K.; Pennycook, S. J.; Pantelides, S. T. Explanation of the observed dearth of three-coordinated Al on gamma-alumina surfaces. *J. Am. Chem. Soc.* **1999**, *121*, 10999−11001.
(25) John, C. S.; Alma, N. C. M.; Hays, G. R. Characterization of Transitional Alumina by Solid-State Magic Angle Spinning Aluminum NMR. *Appl. Catal.* **1983**, *6*, 341−346.
(26) Rozita, Y.; Brydson, R.; Scott, J. An investigation of commercial γ-Al(2)O(3) nanoparticles. *J. Phys. Conf. Ser.* **2010**, *241*, 012096.
(27) Wang, J. A.; Bokhimi, X.; Morales, A.; Novaro, O.; López, T.; Gómez, R. Aluminum local environment and defects in the crystalline structure of sol-gel alumina catalyst. *J. Phys. Chem. B* **1999**, *103*, 299−303.
(28) Menéndez-Proupin, E.; Gutiérrez, G. Electronic properties of bulk γ-Al_2O_3. *Phys. Rev. B: Condens. Matter Mater. Phys.* **2005**, *72*, 035116.
(29) Paglia, G.; Buckley, C. E.; Rohl, A. L.; Hart, R. D.; Winter, K.; Studer, A. J.; Hunter, B. A.; Hanna, J. V. Boehmite derived γ-alumina system. 1. Structural evolution with temperature, with the identification and structural determination of a new transition phase, γ-alumina. *Chem. Mater.* **2004**, *16*, 220−236.
(30) Taniike, T.; Tada, M.; Morikawa, Y.; Sasaki, T.; Iwasawa, Y. Density functional theoretical calculations for a Co-2/γ-Al_2O_3 model catalyst: Structures of the γ-Al_2O_3 bulk and surface and attachment sites for Co2+ ions. *J. Phys. Chem. B* **2006**, *110*, 4929−4936.
(31) Chen, Y.; Ouyang, C.; Shi, S.; Sun, Z.; Song, L. Density functional theory study of Ir atom deposited on γ-Al_2O_3 (001) surface. *Phys. Lett. A* **2009**, *373*, 277−281.
(32) Ahuja, R.; Osorio-Guillen, J. M.; Almeida, J. S. De; Holm, B.; Ching, W. Y.; Johansson, B. Electronic and optical properties of gamma-Al2O3 from ab initio theory. *J. Phys.: Condens. Matter* **2004**, *16*, 2891−2900.
(33) Dabrowski, J.; Butt, J.; Bliss, H. Monte Carlo Simulation of a Catalytic Surface: Activity and Selectivity of y-Alumina for Dehydration. *J. Catal.* **1970**, *18*, 297−313.
(34) Al-Abadleh, H. A.; Grassian, V. H. FT-IR study of water adsorption on aluminum oxide surfaces. *Langmuir* **2003**, *19*, 341−347.
(35) Lefèvre, G.; Duc, M.; Lepeut, P.; Caplain, R.; Fédoroff, M. Hydration of gamma-alumina in water and its effects on surface reactivity. *Langmuir* **2002**, *18*, 7530−7537.
(36) Raybaud, P.; Digne, M.; Iftimie, R.; Wellens, W.; Euzen, P.; Toulhoat, H. Morphology and surface properties of boehmite (gamma-AlOOH): A density functional theory study. *J. Catal.* **2001**, *201*, 236−246.
(37) Kelber, J. A. Alumina surfaces and interfaces under non-ultrahigh vacuum conditions. *Surf. Sci. Rep.* **2007**, *62*, 271−303.
(38) Zamora, M.; Cordoba, A. A study of surface hydroxyl groups on gamma-alumina. *J. Phys. Chem.* **1978**, *82*, 584−588.
(39) Sankara Raman, S.; Nampoori, V. P. N.; Vallabhan, C. P. G.; Ambadas, G.; Sugunan, S. Photoacoustic study of the effect of hydroxyl ion on thermal diffusivity of gamma alumina. *J. Appl. Phys.* **1999**, *85*, 1987.
(40) Bhasin, M. M.; Curran, C.; John, G. S. Infrared study of the effect of surface hydration on the nature of acetylenes adsorbed on gamma-alumina. *J. Phys. Chem.* **1970**, *74*, 3973.
(41) Arrouvel, C.; Digne, M.; Breysse, M.; Toulhoat, H.; Raybaud, P. Effects of morphology on surface hydroxyl concentration: a DFT comparison of anatase-TiO2 and gamma-alumina catalytic supports. *J. Catal.* **2004**, *222*, 152−166.
(42) Ionescu, A.; Allouche, A.; Aycard, J. P.; Rajzmann, M.; Hutschka, F. Study of gamma- alumina surface reactivity: Adsorption of water and hydrogen sulfide on octahedral aluminum sites. *J. Phys. Chem. B* **2002**, *106*, 9359−9366.
(43) Peri, J. B. A Model for the Surface of γ-Alumina. *J. Phys. Chem.* **1965**, *69*, 220−230.
(44) Knözinger, H.; Ratnasamy, P. Catalytic Aluminas: Surface Models and Characterization of Surface Sites. *Catal. Rev.: Sci. Eng.* **1978**, *17*, 31−70.
(45) Hindin, S. G.; Weller, S. W. The Effect of Pretreatment on the Activity of Gamma-Alumina. I. Ethylene Hydrogenation. *J. Phys. Chem.* **1956**, *60*, 1501−1506.
(46) Digne, M.; Sautet, P.; Raybaud, P.; Euzen, P.; Toulhoat, H. Use of DFT to achieve a rational understanding of acid-basic properties of gamma-alumina surfaces. *J. Catal.* **2004**, *226*, 54−68.
(47) Fleisher, M. B.; Golender, L. O.; Shimanskaya, M. V. Electronic Charge-Distribution and Lewis Acidity Of Surface Aluminum Atoms In Gamma-Al2O3 - A Quantum-Chemical Model. *J. Chem. Soc., Faraday Trans.* **1991**, *87*, 745.
(48) Fleisher, M. B.; Shimanskaya, M. V. Quantum Chemical Investigation of Adsorptive Weakening Of Surface Bonds In Gamma-Al2O3 Catalyst. *React. Kinet. Catal. Lett.* **1992**, *48*, 239−245.
(49) Hendriksen, B.; Pearce, D. R.; Rudham, R. Heats of adsorption of water on α- and γ-alumina. *J. Catal.* **1972**, *24*, 82−87.
(50) Ballinger, T. H.; Yates, J. T. IR-Spectroscopic Detection of Lewis Acid Sites On Al2O3 Using Adsorbed Co - Correlation With Al-OH Group Removal. *Langmuir* **1991**, *7*, 3041−3045.
(51) Coster, D.; Blumenfeld, A. L.; Fripiat, J. J. Lewis Acid Sites and Surface Aluminum in Aluminas and Zeolites: A High-Resolution NMR Study. *J. Phys. Chem.* **1994**, *98*, 6201−6211.
(52) Flockhart, B. D.; Scott, J. A. N.; Pink, R. C. Electron-transfer at alumina surfaces. Part 1.- Electron-Acceptor Properties of Aluminas. *Trans. Faraday Soc.* **1966**, *62*, 730−740.
(53) Saniger, J. M. Al-O Infrared Vibrational Frequencies of Gamma-Alumina. *Mater. Lett.* **1995**, *22*, 109−113.
(54) Datta, A. Evidence for cluster sites on catalytic alumina. *J. Phys. Chem.* **1989**, *93*, 7053−7054.
(55) Wischert, R.; Laurent, P.; Copéret, C.; Delbecq, F.; Sautet, P. gamma-Alumina: The Essential and Unexpected Role of Water for the Structure, Stability, and Reactivity of "Defect" Sites. *J. Am. Chem. Soc.* **2012**, *134*, 14430−14449.
(56) Ma, Q.; Liu, Y.; He, H. Synergistic Effect between NO_2 and SO_2 in Their Adsorption and Reaction on γ-Alumina. *J. Phys. Chem. A* **2008**, *112* (29), 6630−6635.
(57) Huang, Z.; Zhang, Z.; Kong, W.; Feng, F.; Qiu, Y.; Tang, S.; Xia, C.; Ma, L.; Luo, M.; Xu, D. Synergistic effect among Cl_2, SO_2 and NO_2 in their heterogeneous reactions on gamma-alumina. *Atmos. Environ.* **2017**, *166*, 403−411.
(58) Karim, W.; Spreafico, C.; Kleibert, A.; Gobrecht, J.; VandeVondele, J.; Ekinci, Y.; van Bokhoven, J. A. Catalyst support effects on hydrogen spillover. *Nature* **2017**, *541*, 68−71.
(59) Cai, S.-H.; Rashkeev, S. N.; Pantelides, S. T.; Sohlberg, K. Atomic Scale Mechanism of the Transformation of γ-Alumina to θ-Alumina. *Phys. Rev. Lett.* **2002**, *89*, 235501.
(60) Tsyganenko, A. A.; Mardilovich, P. P. Structure of alumina surfaces. *J. Chem. Soc., Faraday Trans.* **1996**, *92*, 4843.
(61) Giannozzi, P.; Baroni, S.; Bonini, N.; Calandra, M.; Car, R.; Cavazzoni, C.; Ceresoli, D.; Chiarotti, G. L.; Cococcioni, M.; Dabo, I.; et al. QUANTUM ESPRESSO: a modular and open-source software project for quantum simulations of materials. *J. Phys.: Condens. Matter* **2009**, *21*, 395502.
(62) Wolverton, O.; Hass, K. C. Phase stability and structure of spinel-based transition aluminas. *Phys. Rev. B: Condens. Matter Mater. Phys.* **2001**, *63*, 024102.

DOI: 10.1021/acs.jpcc.8b06506
J. Phys. Chem. C 2018, 122, 25314−25330

(63) Digne, M.; Sautet, P.; Raybaud, P.; Toulhoat, H.; Artacho, E. Structure and Stability of Aluminum Hydroxides: A Theoretical Study. *J. Phys. Chem. B* **2002**, *106*, 5155−5162.
(64) Samain, L.; Jaworski, A.; Edén, M.; Ladd, D. M.; Seo, D. K.; Javier Garcia-Garcia, F.; Häussermann, U. Structural analysis of highly porous γ-Al2O3. *J. Solid State Chem.* **2014**, *217*, 1−8.
(65) Loyola, C.; Menéndez-Proupin, E.; Gutiérrez, G. Atomistic study of vibrational properties of γ-Al_2O_3. *J. Mater. Sci.* **2010**, *45*, 5094−5100.
(66) Ferreira, A. R.; Martins, M. J. F.; Konstantinova, E.; Capaz, R. B.; Souza, W. F.; Chiaro, S. S. X.; Leitão, A. A. Direct comparison between two -γ-alumina structural models by DFT calculations. *J. Solid State Chem.* **2011**, *184*, 1105−1111.
(67) Bermudez, V. M. Quantum-Chemical Study of the Adsorption of DMMP and Sarin on γ-Al_2O_3. *J. Phys. Chem. C* **2007**, *111*, 3719−3728.
(68) Liu, X.; Truitt, R. E. DRFT-IR Studies of the Surface of γ-Alumina. *J. Am. Chem. Soc.* **1997**, *119*, 9856−9860.
(69) Ealet, B.; Elyakhloufi, M. H.; Gillet, E.; Ricci, M. Electronic and crystallographic structure of γ-alumina thin films. *Thin Solid Films* **1994**, *250*, 92−100.
(70) Schiffino, R. S.; Merrill, R. P. A mechanistic study of the methanol dehydration reaction on gamma-alumina catalyst. *J. Phys. Chem.* **1993**, *97*, 6425−6435.
(71) Dyan, A.; Cenedese, P.; Dubot, P. Physical Properties of γ Alumina Surface Hydroxyls Revisited through a Large Scale Periodic Quantum-Chemistry Approach. *J. Phys. Chem. B* **2006**, *110*, 10041−10050.
(72) Fleisher, M. B.; Golender, L. O.; Shimanskaya, M. V. On the mechanism of water dissociation on the surface of Al_2O_3. Quantum-chemical calculations. *React. Kinet. Catal. Lett.* **1992**, *46*, 173−178.
(73) Fleisher, M. B.; Golender, L. O.; Shimanskaya, M. V. Mo CNDO/2 studies of NH_3 adsorption on Lewis acidic sites ofγ-Al_2O_3 surface. *React. Kinet. Catal. Lett.* **1984**, *24*, 25−29.
(74) Arrouvel, C.; Breysse, M.; Toulhoat, H.; Raybaud, P. A density functional theory comparison of anatase (TiO2)- and γ-Al2O3-supported MoS2 catalysts. *J. Catal.* **2005**, *232*, 161−178.
(75) Arrouvel, C.; Toulhoat, H.; Breysse, M.; Raybaud, P. Effects of PH2O, PH2S, PH2 on the surface properties of anatase−TiO2 and γ-Al2O3: a DFT study. *J. Catal.* **2004**, *226*, 260−272.
(76) Fleisher, M. B.; Golender, L. O.; Shimanskaya, M. V. A quantum-chemical study of indirect interactions between adsorbate molecules on γ-Al_2O_3 catalyst. *React. Kinet. Catal. Lett.* **1988**, *36*, 441−446.
(77) Fiorentini, V.; Methfessel, M. Extracting convergent surface energies from slab calculations. *J. Phys.: Condens. Matter* **1996**, *8*, 6525−6529.
(78) McHale, J. M.; Auroux, A.; Perrotta, A. J.; Navrotsky, A. Surface Energies and Thermodynamic Phase Stability in Nanocrystalline Aluminas. *Science* **1997**, *277*, 788−791.
(79) Castro, R. H. R.; Ushakov, S. V.; Gengembre, L.; Gouvêa, D.; Navrotsky, A. Surface Energy and Thermodynamic Stability of γ-Alumina: Effect of Dopants and Water. *Chem. Mater.* **2006**, *18*, 1867−1872.
(80) Boettger, J. C. Nonconvergence of surface energies obtained from thin-film calculations. *Phys. Rev. B: Condens. Matter Mater. Phys.* **1994**, *49*, 16798.
(81) Peri, J. B.; Hannan, R. B. Surface Hydroxyl Groups On γ-Alumina. *J. Phys. Chem.* **1960**, *64*, 1526−1530.
(82) Potdar, H. S.; Jun, K. W.; Bae, J. W.; Kim, S. M.; Lee, Y. J. Synthesis of nano-sized porous γ-alumina powder via a precipitation/digestion route. *Appl. Catal., A* **2007**, *321*, 109−116.
(83) Zabka, W. D.; Leuenberger, D.; Mette, G.; Osterwalder, J. From two- to three-dimensional alumina: Interface templated films and formation of γ-Al_2O_3(111) nuclei. *Phys. Rev. B: Condens. Matter Mater. Phys.* **2017**, *96*, 155420.
(84) Cococcioni, M.; de Gironcoli, S. Linear response approach to the calculation of the effective interaction parameters in the LDA+U method. *Phys. Rev. B: Condens. Matter Mater. Phys.* **2005**, *71*, 035105.

DOI: 10.1021/acs.jpcc.8b06506
J. Phys. Chem. C 2018, 122, 25314−25330